STUDY REPORT

No. 92 (revised 2004)

BRANZFIRE Technical Reference Guide

C.A. Wade

The work reported here was funded by the Foundation for Research, Science and Technology from the Research for Industry Fund and by Building Research Association of New Zealand Inc from the Building Research Levy.

Preface

This report describes the underlying physics and assumptions used in developing the computer software model *BRANZFIRE*.

Acknowledgments

Thanks and appreciation are due to the many people who have contributed to the development of BRANZFIRE both directly and indirectly. There are now too many to mention here by name but their efforts have been very much appreciated.

The work reported here was funded by the Foundation for Research, Science and Technology, New Zealand from the Research for Industry Fund and by BRANZ Inc from the Building Research Levy.

Note

This report is intended for users of the BRANZFIRE software.

BRANZFIRE Technical Reference Guide 2004

REFERENCE

C.A.Wade (2004). BRANZFIRE Technical Reference Guide 2004. BRANZ Study Report 92 (revised). Building Research Association of New Zealand. Judgeford, Porirua City, New Zealand.

ABSTRACT

This report describes the assumptions and underlying physics upon which the computer fire model *BRANZFIRE* version 2004 is based. The software is intended for evaluating the performance and hazard associated with room fires including combustible room lining materials. It comprises a multi-room zone model fully integrated or coupled with flame spread and fire growth models applicable to room fire scenarios. In particular, it is intended to simulate ISO 9705 room corner fire tests. The fire growth models use fire property data obtained from a cone calorimeter as input. Model output includes but is not limited to: gas layer temperatures, pressure, room surface temperatures, layer height, visibility and fractional effective dose estimates.

Keywords :- COMPUTER MODELS; FIRE GROWTH; FIRE HAZARD; FIRE MODELS; FIRE SAFETY; FIRE SPREAD; FLAME SPREAD; HAZARD ASSESSMENT; MATERIAL PROPERTIES; SMOKE FILLING; SMOKE LAYERS; TESTS.

Contents

List of Tables

List of Figures

Section 1

Nomenclature

a	=	gas absorption coefficient (m^{-1})
A	=	plume entrainment coefficient
A_f	=	floor area of the room (m^2)
A_i	=	area of the i^{th} surface (m^2)
A_p	=	pyrolysis area (m^2)
A_{p1}	=	pyrolysis area on wall (m^2)
A_{pj1}	=	pyrolysis area on wall in ceiling jet region (m^2)
A_{pc1}	=	pyrolysis area on ceiling (m^2)
A_w	=	wall area behind burner (m^2)
A_o	=	initial pyrolysing area in ceiling (m^2)
Bi	=	Biot Number
Bi_{int}	=	Biot Number for the room interior surface
Bi_{ext}	=	Biot Number for the room exterior surface
b_w	=	side dimension of square burner (m)
c	=	specific heat (J/kg K)
c_p	=	specific heat of air (J/kg K)
C	=	sprinkler conduction factor
C_{soot}	=	mass concentration of soot in the upper layer (kg soot/m^3)
D	=	diameter of the fire (m)
D_i	=	smoke optical density inside the detector (m^{-1})
D_o	=	smoke optical density outside the detector (m^{-1})
$F_{i,j}$	=	geometric configuration factor for radiation emitted from surface i and intercepted by surface j
FED	=	fractional effective dose
Fo	=	Fourier Number
g	=	gravitation constant (m/s^2)

Gr	=	grashof number
h	=	heat transfer coefficient (W/m^{2}K)
h_c	=	convective heat transfer coefficient (W/m^{2}K)
h_v	=	vent height (m)
h_{ig}	=	total heat transfer coefficient from surface at ignition (W/m^{2}K)
H	=	height of the ceiling above the base of the fire (m)
$\dot{H}_l$	=	enthalpy flow to the lower layer (kW)
$\dot{H}_u$	=	enthalpy flow to the upper layer (kW)
k	=	thermal conductivity (W/mK)
k_{avg}	=	average extinction coefficient (m^{-1})
k_m	=	particle extinction cross-section (m^2 /kg soot)
k_s	=	effective absorption coefficient of soot
$k\rho c$	=	thermal inertia (W^{2}s/m^{4}K^2)
K	=	flame area constant (m^2/kW)
l	=	characteristic dimension (m)
L	=	flame height (m)
L_g	=	heat of gasification (kJ/g)
L_o	=	mean path length (m)
$\dot{m}_d$	=	mass flow rate in vent mixing flow (kg/s)
$\dot{m}_f$	=	mass loss rate of the fuel (kg/s)
$\dot{m}''_f$	=	mass loss rate of fuel per unit area (kg/s m^2)
$\dot{m}_i$	=	mass flow rate of cool gases in through the vent (kg/s)
$\dot{m}_o$	=	mass flow rate of hot gases out through the vent (kg/s)
$\dot{m}_p$	=	mass flow rate of air entrained into the plume (kg/s)
M_l	=	mass of the lower layer (kg)
M_u	=	mass of the upper layer (kg)
MW_i	=	molecular weight of species i
n	=	flame length power
ppm	=	parts per million
p	=	horizontal flame projection distance (m)
P_a	=	atmospheric pressure (kPa)
P	=	pressure in the room at floor level relative to atmospheric (Pa)
P_i	=	partial pressure of species i (kPa)
P_{ws}	=	saturation pressure for water vapor (kPa)
Pr	=	prandtl number
$\dot{q}''$	=	heat flux per unit area (kW/m^2)
$\dot{q}''_{\mathrm{cr}}$	=	critical heat flux for ignition (kW/m^2)
$\dot{q}''_e$	=	external heat flux incident on a surface (kW/m^2)

$\dot{q}''_w$ = net heat flux from the burner flame to a wall (kW/m^2)
$\dot{q}''_f$ = net heat flux from the flame impinging on ceiling (kW/m^2)
$\dot{q}_l$ = net heat transfer to the lower gas layer (kW)
$\dot{q}''_{\rm int}$ = incident heat flux to a surface due to gas layers and other surfaces (kW/m^2)
$\dot{q}''_{\rm net}$ = net heat flux to a surface (kW/m^2)
$\dot{q}''_{ff}$ = heat flux ahead of the flame (kW/m^2)
$\dot{q}''_r$ = radiative component of heat flux (kW/m^2)
$\dot{q}_u$ = net heat transfer to the upper gas layer (kW)
q''_{f-k} = heat flux striking the $k^{\rm th}$ surface due to a point source fire (kW)
$q''^{\rm i,gas}_{j-k}$ = heat flux striking the $k^{\rm th}$ surface due to emitting $i^{\rm th}$ gas layer (kW)
$\dot{Q}''(t)$ = time dependent heat release rate measured in cone calorimeter (kW/m^2)
$\dot{Q}''$ = heat release rate (kW/m^2)
$\dot{Q}_b$ = heat release rate of the gas burner (kW)
$\dot{Q}'_b$ = heat release rate per unit length of the gas burner (kW)
$\dot{Q}_c$ = convective heat release from the fire (kW)
$\dot{Q}''_c(t)$ = time dependent heat release rate measured in cone calorimeter (kW/m^2)
$\dot{Q}_f$ = total heat release from the fire (kW)
$\dot{Q}''_{\rm p,cone}$ = peak rate of heat release measured in cone calorimeter test (kW/m^2)
$\dot{Q}_p$ = peak heat release (kW/m^2)
$\dot{Q}(t)$ = heat release at time t (kW)
$\dot{Q}(t_{\rm act})$ = heat release rate at the time of sprinkler activation (kW)
r = radial distance from the centre of the plume (m)
R = universal gas constant (J/kmol/K)
RMV = volume of air breathed (liters/min)
RTI = response time index (ms$^{1/2}$)
SA = surface area of a flame volume (m^2)
t = time (sec)
$t_{\rm act}$ = sprinkler activation time (sec)
$t_{\rm ig}$ = time to ignition in cone calorimeter (sec)
t_h = time for y pyrolysis front to reach ceiling (sec)
t_p = dummy variable of integration
T = temperature (K)
$T_{\rm cj}$ = temperature of the ceiling jet (K)
$T_{\rm ig}$ = surface temperature for ignition (K)
T_e = temperature of detector/sprinkler link (K)
T_f = flame temperature (K)
$T_{\rm fo}$ = flashover temperature (K)
T_g = gas temperature (K)

T_o	=	initial surface temperature (K)
T_l	=	temperature of the lower gas layer (K)
T_u	=	temperature of the upper gas layer (K)
T_i	=	temperature of the i^{th} gas layer (K)
T_m^p	=	temperature of node m at time p (K)
T_s	=	surface temperature (K)
$T_{\text{s,min}}$	=	minimum surface temperature for spread (K)
T_∞	=	reference temperature of ambient air (K)
U_{cj}	=	velocity of the ceiling jet (m/s)
V	=	visibility in upper layer (m)
$V_a(t)$	=	velocity of the pyrolysis front (m^2/sec)
V_l	=	volume of the lower layer (m^3)
V_u	=	volume of the upper layer (m^3)
V_R	=	volume of the room (m^3)
w	=	vent width (m)
w_o	=	width to which vent flow expands to (m)
$\dot{w}''$	=	water spray density (mm/s)
W_s	=	humidity ratio of air at saturation
x_p	=	pyrolysis front in lateral direction (m)
$x_{p,o}$	=	initial pyrolysis front in lateral direction (m)
X_f	=	position of the flame front (m)
y_f	=	flame length in upward direction (m)
y_p	=	pyrolysis front in upward direction (m)
$y_{p,o}$	=	initial pyrolysis front in upward direction (m)
$Y_{i,l}$	=	mass fraction of species i in the lower layer
$Y_{i,u}$	=	mass fraction of species i in the upper layer
$Y_{i,\infty}$	=	mass fraction of species i in ambient air
Y_{soot}	=	mass fraction of soot in the upper layer
z_p	=	pyrolysis front in downward direction from ceiling jet (m)
Z	=	height of the smoke layer from the base of the fire (m)
Z_o	=	virtual origin (m)
Z_n	=	height of the neutral plane (m)
$\%\text{COHb}$	=	concentration of carboxyhemoglobin in the blood
α	=	thermal diffusivity (m^2/s)
α_t	=	total absorptance of gas-soot mixture
α_{j-k}^i	=	absorptivity of i^{th} gas layer for a path between surfaces j and k
ϵ	=	emissivity
ϵ_t	=	total emissivity of gas-soot mixture

ρ	=	density (kg/m^3)
$\delta_{k,j}$	=	kronecker delta function
γ	=	c_p/c_v
ρ_l	=	density of the lower layer (kg/m^3)
ρ_u	=	density of the upper layer (kg/m^3)
λ_r	=	radiative fraction of energy loss by radiation from the flame/plume
ϕ	=	radiation configuration factor
ν	=	kinematic viscosity
Φ	=	flame spread parameter (kW^2/m^3)
Φ_e	=	global equivalence ratio
Φ_{RH}	=	relative humidity
ω_{f-k}	=	solid angle between k^{th} surface and a point source fire
σ	=	Stefan Boltzmann constant ($= 5.67 \times 10^{-8}$ W/m^{2}K^4)
τ	=	time constant for the detector (sec)
τ	=	time to ignition (sec)
τ_t	=	radiation transmission factor
τ_w	=	time to ignition of the wall lining (sec)
τ^i_{j-k}	=	transmissivity of i^{th} gas layer for a path between surfaces j and k
Ψ_i	=	yield of species i from the pyrolysing fuel (kg species i/kg fuel)
Ψ_{soot}	=	yield of soot from the pyrolysing fuel (kg soot/kg fuel)
ΔA_p	=	incremental change in pyrolysis area (m^2)
Δt	=	time step (sec)
ΔH_c	=	heat of combustion (kJ/g)
Δx	=	incremental surface thickness for heat conduction calculation (m)

Section 2

Introduction

BRANZFIRE [1, 2, 3, 4] is a computer fire model which integrates a flamespread and fire growth model for room lining materials with a multi-room zone model. Its purpose is to model fire hazard associated with combustible room lining materials and building contents, and to quantify their contribution to the rate of fire development within and between rooms.

BRANZFIRE was originally developed by the author while studying for a Master of Science in Fire Protection Engineering at Worcester Polytechnic Institute, USA during 1994-95. Since then development has continued at BRANZ Ltd funded by the Foundation for Research Science and Technology and by BRANZ Inc from the Building Research Levy.

Programming is carried out using Microsoft Visual Basic 6.0, and the software requires Microsoft Windows 95, 98, 2000, XP or Windows NT 3.51 or later. This guide has been written for BRANZFIRE version 2004.

Section 3

BRANZFIRE - Fire Growth Model

BRANZFIRE includes a flamespread and fire growth model principally for the room-corner fire scenario. The fire growth model is based on the work of Quintiere [5] and accounts for both wind-aided and opposed flow flame spread. A number of improvements and modifications to the original Quintiere model have been made as will be described in this guide.

3.1 Quintiere's Room-Corner Model

This flame spread and fire growth model is generally based on previous work by Quintiere [5]. BRANZFIRE predicts ignition, flame spread and the resultant heat released by the wall and ceiling lining material. Two modes of flame spread are considered. Upward flame spread includes the spread beneath the ceiling and along the wall/ceiling intersection in the region of the ceiling jet. The opposed flow flame spread includes lateral flame spread on the wall and downward spread from the ceiling jet.

While Quintiere's model has been used as the basis of the model described here, a number of significant modifications and changes have been incorporated. These include:

- Assuming a non-uniform burning rate based on time-dependent heat release rate data measured in a cone calorimeter.
- Only the upward, not lateral, burnout front is solved for.
- Estimating the flame flux from a burning object to the wall as described in the next section. Quintiere originally assumed 60 kW/m^2. The wall region first ignited is assumed to be bounded by the calculated flame height and the side dimensions of the burner.
- Assuming the flame flux in the pyrolysing regions (but outside the burner region) is 35 kW/m^2 as discussed later, while the assumed flame flux ahead of the flame front (ie regions not yet ignited but subject to preheating) is assumed to be 30 kW/m^2. A new correlation is used to estimate the heat flux from the burner flame to the surfaces depending on the heat output of the burner.

- Determining the surface temperatures for the wall and ceiling using a finite difference method with the upper layer temperature as a boundary condition. The upper layer temperature is determined from a mass and energy balance for the room. As a result, an upper layer temperature correlation is not used.
- Adding subroutines to account for the direct ignition of the ceiling lining (independent of wall ignition).

3.1.1 Characterising the burner

In the ISO 9705 room-corner test [6], the wall is ignited with a propane gas burner of output 100 kW for the first 600 seconds which is then increased to 300 kW until completion of the test at 1200 seconds.

The height of the burner flame, L, in the room-corner test is determined using a correlation from Lattimer [7].

$$L/b_w = 5.9Q^{*1/2} \tag{3.1}$$

where $\dot{Q}^* = \dot{Q}_b/(1110{b_w}^{5/2})$ and b_w is the width of one side of a square burner.

The burner may also be located against a wall or in the centre of the room as well as in a room corner. This has been allowed for by selecting correlations for the burner flame height appropriate to the burner position. The Heskestad correlation for a burner located in the centre of the room is [8]:

$$L = -1.02D + 0.235\dot{Q}_b^{2/5} \tag{3.2}$$

The same flame height correlation is also used when the burner is placed against a wall.

Heat flux correlations for a fire in the corner of a room were also developed by Lattimer [7]. Along the height of the wall, the peak heat flux to the wall is given as a function of the burner dimension by:

$$\dot{q}''_w = 120[1 - e^{-4.0b_w}] \tag{3.3}$$

The maximum heat flux to the ceiling in the corner (at the point of impingement) was given by:

$$\dot{q}''_c = 120 \text{ for } H/L \leq 0.52 \tag{3.4}$$

$$\dot{q}''_c = 13H/L^{-3.5} \text{ for } H/L > 0.52 \tag{3.5}$$

The method for determining the heat flux from the burner flame against a flat wall is based on work by Back et al [9]. They developed a correlation based on square propane burners against a wall. The burners varied in output from 50-500 kW and had edge lengths of 0.28 to 0.7 m. The maximum heat flux incident to the wall from the burner flame is given by:

$$\dot{q}''_w = E(1 - e(-k\dot{Q}_b^{1/3})) \tag{3.6}$$

Where $E = 200$ kW/m^2 and $k = 0.09$ kW$^{-1/3}$. This heat flux was assumed to be constant over the wall area up to the height of the flame. Above the flame height, the heat flux reduces with height (Z) according to:

$$\dot{q}''_w = 20(Z/L)^{-5/3} \tag{3.7}$$

This latter equation is relevant for estimating the heat flux at ceiling level prior to ignition of the wall.

3.1.2 Ignition of the wall lining

There are two methods for determining the ignition time for the wall depending on which ignition data correlation has been selected. When the Flux Time Product (FTP) method [10] is used then the time for the wall lining to ignite (t_{ig}) is that time after which the Flux Time Product for the material has exceeded the FTP$_n$ value determined from the correlation of the cone calorimeter ignition data as described in section 5.2 and expressed by the equation below.

$$FTP_n = \int_0^{t_{ig}} (\dot{q}''_e - \dot{q}''_{cr}) \text{ where } \dot{q}''_e > \dot{q}''_{cr} \tag{3.8}$$

The incident heat flux exposing the wall $\dot{q}''_e$ in the region of the burner flame, $\dot{q}''_{\text{net}}$, is given by summing the incident heat flux from the flame, $\dot{q}''_w$, and the incident heat flux due to the heated gas layers and other room surfaces, $\dot{q}''_{int}$ as follows:

$$\dot{q}''_{\text{net}} = \dot{q}''_w + \dot{q}''_{int} \tag{3.9}$$

When the Grenier and Janssens method [11] of correlating the ignition data is selected then a finite difference scheme is used to determine the surface temperature of the wall lining, and the wall is ignited when the ignition temperature is reached.

3.1.3 Upper layer gas temperature

The upper layer temperature correlation as used by Quintiere [5] is not used here since the zone model calculates the time dependent upper layer gas temperature as described later in Section 4.2.

3.1.4 Energy release rate - Method 1

Two methods are provided for determining the heat released over time by the surface lining materials. The first (Method 1) uses cone calorimeter test data obtained at only

a single heat flux, while the second (Method 2) uses cone calorimeter test data obtained uding a range of exernal heat fluxes. Method 2 is recommended to the user whenever possible.

Method 1 estimates the energy release rate from burning room lining materials based on the input of cone calorimeter data at a single heat flux and extrapolates to estimate the energy release at different imposed heat fluxes.

The peak heat release rate per unit area for the lining material is estimated, as generally described by Quintiere, as follows:

$$\dot{Q}''_p = \frac{\Delta H_c}{L_g}(\dot{q}''_w + \dot{q}''_{\rm int} - \epsilon\sigma T^4_{\rm ig}) \tag{3.10}$$

where $\dot{q}''_w$ is the applicable flame heat flux over the pyrolysis region, $\dot{q}''_{\rm int}$ is the heat flux from the hot gas layer and other room surfaces (excluding the reradiation term), and $T_{\rm ig}$ is the assumed temperature of the pyrolysing surface being equal to the ignition temperature of the surface [12] or the surface temperature determined from the zone model, whichever is the higher. ΔH_c is the effective heat of combustion from the cone calorimeter, and L_g is the heat of gasification determined by the model from a correlation of the peak heat release rate data from cone calorimeter experiments.

The model separately considers the pyrolysing region outside the burner flame region from that impinged on by the burner flame. While the burner flame heat flux is calculated as described above, the flame flux to the material outside the burner region is taken as 35 kW/m^2.

The model normalises the input heat release rate curve (from the cone calorimeter) by dividing by the peak heat release rate ($\dot{Q}''_{\rm p,cone}$, from the cone test) at each time step. The value of the peak rate of heat release determined by equation 3.10 is then multiplied by the normalised ratio given that the elapsed time from ignition is known.

$$\dot{Q}''(t) = \frac{\dot{Q}''_c(t)}{\dot{Q}''_{\rm p,cone}}\dot{Q}''_p \tag{3.11}$$

The model also makes a transformation of the new heat release rate curve by scaling the time axis so that the total area under the curve (total energy available) remains the same as that measured in the cone calorimeter test. This is illustrated in Figure 3.1.

The total energy released is the sum of that from the burner, the walls and the ceiling and this is given by:

$$\dot{Q}(t) = \dot{Q}_b + \Sigma(\dot{Q}''(t)\Delta A_p(t)) \tag{3.12}$$

where $\dot{Q}_b$ is the heat release rate of the burner, $\dot{Q}''(t)$ is the heat release rate per unit area from the lining material at time t, and ΔA_p is the incremental pyrolysis area. At each timestep the pyrolysis area is calculated as described below, and the timestep at which each incremental area first ignited is therefore known. The total heat release rate is the sum of the incremental pyrolysis areas multiplied by the time-dependent heat release rate for each incremental area.

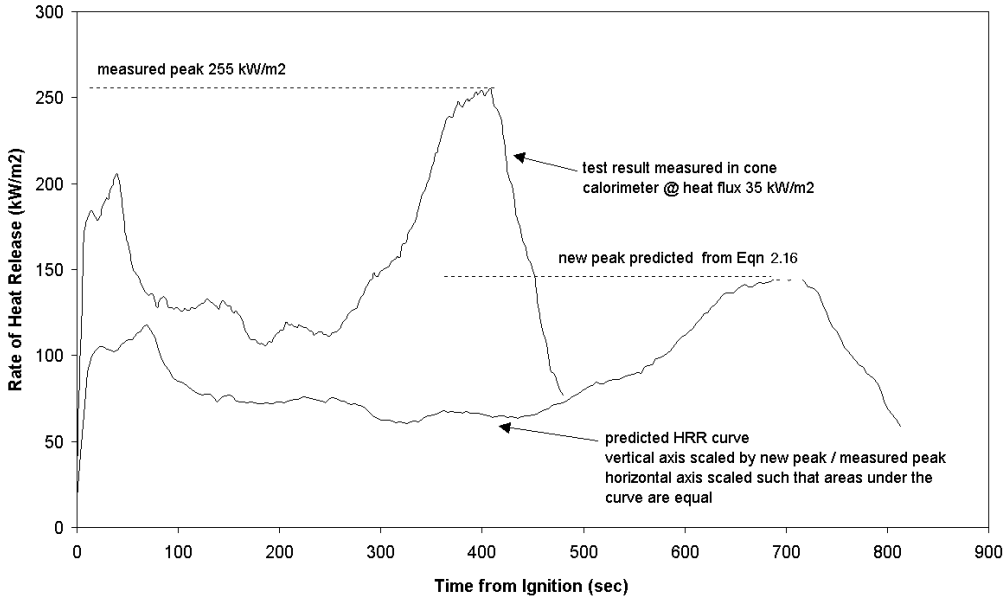

Figure 3.1: Transformation of the heat release rate curve

3.1.5 Energy release rate - Method 2

This method estimates the energy release rate from burning room lining materials based on the input of cone calorimeter data at multiple heat fluxes and interpolates the data to estimate the energy release at a specified imposed heat flux based on the elapsed time since ignition.

The total energy released is the sum of that from the burner, the walls and the ceiling and this is given by:

$$\dot{Q}(t) = \dot{Q}_b + \Sigma(\dot{Q}''(t)\Delta A_p(t)) \tag{3.13}$$

where $\dot{Q}''$ is the energy release per unit area for each incremental area and depends on the elapsed time of burning for each incremental area. This is determined from the available set of cone calorimeter heat release rate curves for the material determined for a range of external heat fluxes. The data set is interpolated using a cubic spline technique [13] to determine the applicable energy release rate given the elapsed time from ignition, and the imposed heat flux to the wall. Data is extrapolated, so that where the imposed heat flux is outside the range bounded by the cone calorimeter tests, the energy release rate is estimated by multiplying the data from the the nearest curve by the ratio of the predicted incident flux to the cone curve external flux. $\dot{Q}_b$ is the heat release rate of the burner and ΔA_p is the incremental pyrolysis area. At each timestep the pyrolysis area is calculated as described below, and the timestep at which each incremental area first ignited is therefore known. The total heat release rate is the sum of the incremental pyrolysis areas multiplied by the time-dependent heat release rate for each incremental area.

This method relies on the availability of time-dependent cone calorimeter heat release rate

data for a range of different heat fluxes (typically ranging from 25 to 75 kW/m^2), and is the preferred method.

Determining the pyrolysis area

There are two cases to consider. The first is when the pyrolysis front has not yet reached the ceiling, and the second is when it has. The area calculations are the same as those described by Quintiere [5]. In the first case, the wall adjacent to the burner has ignited and is pyrolysing, while the pyrolysis front has not yet reached the ceiling, as shown in Figure 3.2. The region initially adjacent to the burner is defined by $(x_{p,o}, y_{p,o})$. On ignition of the wall, $x_{p,o} = b_w$ m and $y_{p,o} = 0.4L$ m, where $y_{p,o}$ represents the height of the ignited region above the burner, L is the flame height and $x_{p,o}$ represents the width of the burner.

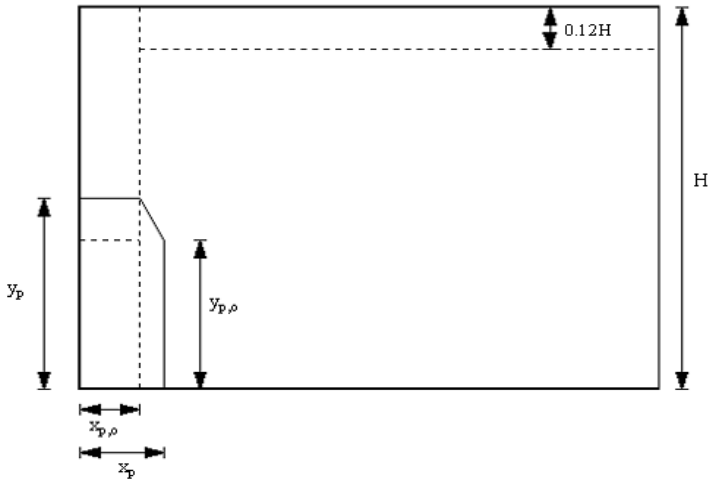

Figure 3.2: Wall ignited; pyrolysis front has not reached the ceiling

The pyrolysis area is given by:

$$A_p = 2\left[y_p x_{p,o} + (x_p - x_{p,o})y_{p,o} + 0.5(y_p - y_{p,o})(x_p - x_{p,o})\right] \tag{3.14}$$

In the second case, the wall adjacent to the burner has ignited and is pyrolysing, and the pyrolysis front has reached the ceiling, as shown in Figure 3.3.

The total pyrolysis area will be the sum of three areas - the wall area A_{p1}, the ceiling jet area A_{pj1}, and the ceiling area A_{pc1}. These required equations are given by:

$$A_{p1} = 2\left[H x_{p,o} + (x_p - x_{p,o})y_{p,o} + 0.5(x_p - x_{p,o})(H - y_{p,o})\right] \tag{3.15}$$

$$z_p = x_p - x_p(t_H) \tag{3.16}$$

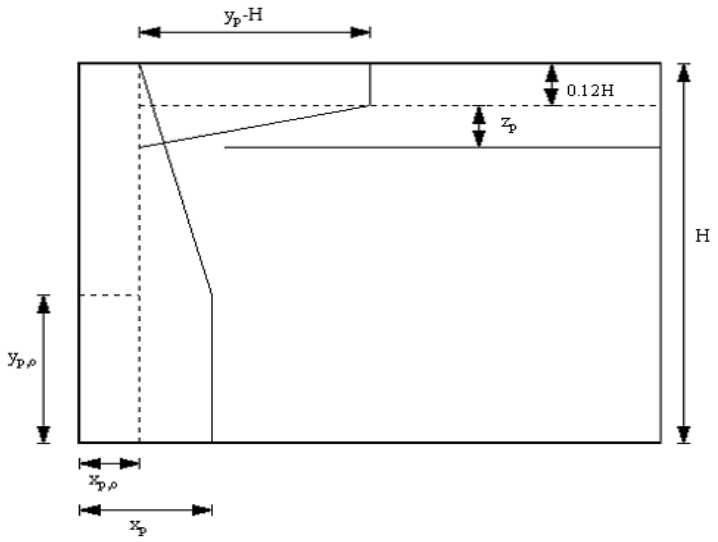

Figure 3.3: Wall ignited; pyrolysis front has reached the ceiling

t_H is the time when the y-pyrolysis front reaches the ceiling.

For $z_p = 0$,

$$A_{pj1} = 2(y_p - H)(0.12H) \tag{3.17}$$

And for $z_p > 0$,

$$A_{pj1} = 2\left[(y_p - H)(0.12H) + 0.5z_p(y_p - H) - 0.5(0.12H + z_p)^2\left(\frac{x_p - x_{p,o}}{H - y_{p,o}}\right)\right] \tag{3.18}$$

$$A_{pc1} = \text{ the lesser of } \frac{\pi}{4(y_p - H)^2} \text{ or the ceiling area} \tag{3.19}$$

$$A_p = A_{p1} + A_{pj1} + A_{pc1} \tag{3.20}$$

The depth of the ceiling jet is taken as 12% of the ceiling height above the burner surface, being an upper end rule-of-thumb estimate from Evans [14].

3.1.6 Upward flame spread

The governing equation for upward flame spread is given by Quintiere as:

$$\frac{dy_p}{dt} = \frac{y_f - y_p}{t_{\text{ig}}} \tag{3.21}$$

where, for thermally thick materials, t_{ig} is given by:

$$t_{\mathrm{ig}} = \frac{\pi}{4} k\rho c \left[\frac{T_{\mathrm{ig}} - T_{\mathrm{s}}}{\dot{q}''_{\mathrm{ff}}} \right]^2 \tag{3.22}$$

The heat flux ahead of the flame, $\dot{q}''_{\mathrm{ff}}$, is assumed to be 30 kW/m^2, while T_{s} is the lining surface temperature and $k\rho c$ is determined as described in section 5.1. y_p is the position of the upward pyrolysis front and y_f is the flame length in the upward direction.

Alternatively, where the FTP method [10] is used to correlate the ignition data, the time to ignition expression used is:

$$t_{\mathrm{ig}} = \mathrm{FTP_n} (\dot{q}''_{\mathrm{ff}} - \dot{q}''_{\mathrm{cr}})^{-1/p} \tag{3.23}$$

For the case where the flames from the wall or ceiling material is contiguous with the burner flame, the flame length y_f is given by equations 3.1 or 3.2 depending on the location of the burner, and with Q taken as the heat release from both the burner and lining material.

The upward burnout front is also modelled to determine the case where the burner flame and wall-ceiling flame are not contiguous or have separated.

$$\frac{dy_b}{dt} = \frac{y_p - y_b}{t_b} \tag{3.24}$$

where y_b is the position of the upward burnout front and t_b is a burnout time (s) and is equal to the area under the heat release rate curve (kJ/m^2) divided by the applicable heat release rate for the lining material (kW/m^2) at a particular time (from the small-scale Cone Calorimeter data).

When $y_b >$ burner flame length, the burner flame and the wall-ceiling flame are assumed to be non-contiguous or separate. In this case the position of the flame front is given by:

$$y_f = y_b + K(\dot{Q}''_p (y_p - y_b))^n \tag{3.25}$$

where K is the flame area constant (=0.0065), n is the flame length power (=1) [15] and $\dot{Q}''_p$ is the heat release rate per unit area for the lining material. When method 1 (section 3.1.4) for determining the energy release rate is used, $\dot{Q}''_p$ is determined from equation 3.10. When method 2 (section 3.1.5) for determining the energy release rate is used, $\dot{Q}''_p$ is determined by interpolation of the peak heat release rates from the cone calorimeter data provided.

In addition, the model allows for the height of the burner above the floor, and takes this into account in the calculations although this is not shown in the above equations. This height is typically 0.3 m for the ISO 9705 burner.

Although the model allows for different lining materials to be specified for the wall and ceiling lining respectively, only one governing upward flame spread rate is calculated. Since the flame spread rate could be influenced by the ceiling material or by that wall material in the ceiling jet region beneath the ceiling, *BRANZFIRE* uses the worse case and thus the material with the lower ignition temperature in the above equations.

3.1.7 Independent ignition of the ceiling lining

BRANZFIRE also allows for separate materials to be specified as the wall and ceiling lining, and therefore there may be instances where the ceiling lining is ignited directly by the fire plume, instead of progressive flame spread originating from the wall lining material. It may also be that a non-combustible or inert material is used for the wall lining so that it would never ignite, thus the possibility of direct ceiling ignition has been considered.

For a corner fire the incident heat flux on the ceiling is determined using equations 3.3 to 3.5 depending on the position of the flame tip in relation to the ceiling. Additional heating by the gas layers and other room surfaces are also added.

For a wall fire the incident heat flux on the ceiling is determined using equation 3.6 if the flame is touching the ceiling or from equation 3.7 if the burner flame is not touching the ceiling. Additional heating by the gas layers and other room surfaces are also added.

$$\dot{Q}''_{\text{ceil}} = \dot{q}''_{w} + \dot{q}''_{\text{int}} \tag{3.26}$$

Following ignition of the ceiling, the pyrolysis area and heat release is determined at each time step. The area first ignited is assumed to be a quarter-circle for a fire in a corner, a semi-circular for a fire against a wall and a full circle for a fire in the centre of the room with a radius of $y_p - H$ in each case (where y_p is measured from the floor and H is the floor to ceiling height).

When the fire is located in the corner or against a wall, the pyrolysis area on the ceiling is compared to the area determined in the previous case involving progressive spread from the wall to the ceiling, and the greater of the two areas is used.

3.1.8 Lateral and downward flame spread

The lateral pyrolysis front is given by:

$$\frac{dx_p}{dt} = \frac{\Phi}{k\rho c(T_{\text{ig}} - T_{\text{s}})^2} \tag{3.27}$$

where Φ is a flame spread parameter. Equation 3.27 is only applicable for $T_{\text{s}} \geq T_{\text{s,min}}$. $T_{\text{s,min}}$ is the minimum surface temperature for spread. Φ and $T_{\text{s,min}}$ are determined from the LIFT test [16].

Section 4

BRANZFIRE - Zone Model

4.1 Introduction

The BRANZFIRE zone model is developed using principles of mass and energy conservation to predict various phenonema associated with room fires. The zone model essentially consists of two homogenous zones, a hot upper layer and a relatively cool lower layer. The fire plume is treated as the mechanism by which the combustion products from the fire and entrained air are transported from the lower layer to the upper layer. The model allows for up to 10 interconnected rooms. A schematic of a fire zone model showing the mass flows into and out of a single compartment is shown in Figure 4.1.

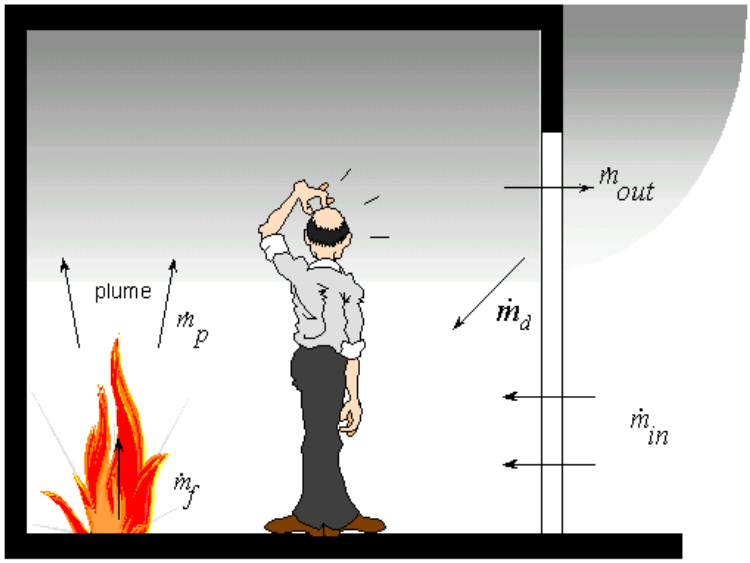

Figure 4.1: Schematic of a zone model

4.2 Mass and Energy Balance

Conservation of mass and energy leads to a set of first order differential equations which allow the upper layer volume, upper and lower layer temperatures, and the pressure equation to be solved.

The form of the equations is as given by Peacock et al [17] for the CFAST model.

The equation for the pressure in the room is:

$$\frac{dP}{dt} = \frac{\gamma - 1}{V_R}(\dot{h}_L + \dot{h}_U) \tag{4.1}$$

The pressure is nominally the pressure at the elevation of the floor, and is relative to the atmospheric pressure at a nominated reference elevation. The offset pressure is used to avoid unnecessary loss of significant digits when solving vent flow equations, where the pressure differences across the vent are very small.

The equation for the volume of the upper layer is:

$$\frac{dV_u}{dt} = \frac{1}{\gamma P}\left[(\gamma - 1)\dot{h}_U - V_u\frac{dP}{dt}\right] \tag{4.2}$$

The lower layer volume is the difference between the room volume (a constant) and the upper layer volume. The height of the smoke layer interface above the floor for a room of uniform area and flat ceiling is then given by:

$$Z = \frac{V_R - V_u}{A_f} \tag{4.3}$$

The ceiling can be specified as flat or sloping. In the latter case, the geometry of the upper volume is taken into account by the model when solving for the position of the layer interface height.

The equation for the temperature of the upper layer is:

$$\frac{dT_u}{dt} = \frac{1}{c_p\rho_u V_u}\left[(\dot{h}_u - c_p\dot{M}_u T_u) + V_u\frac{dP}{dt}\right] \tag{4.4}$$

The equation for the temperature of the lower layer is:

$$\frac{dT_l}{dt} = \frac{1}{c_p\rho_l V_l}\left[(\dot{h}_l - c_p\dot{M}_l T_l) + V_l\frac{dP}{dt}\right] \tag{4.5}$$

The convective enthalpy of the fire $\dot{Q}_f$ includes that from the burner/source, the burning wall lining and the ceiling lining. In the case of a room-corner fire, the fire is represented by a single fire plume. The description of the mass flow in the plume is given later in section 4.6.

The equations for the rate of change of mass in the upper and lower layers are given by:

$$\frac{dM_u}{dt} = \dot{m}_p + \dot{m}_f - \dot{m}_d - \dot{m}_o + \dot{m}_w \tag{4.6}$$

$$\frac{dM_l}{dt} = \dot{m}_i + \dot{m}_d - \dot{m}_p - \dot{m}_w \tag{4.7}$$

The mass from the fuel includes the burner/source, wall and ceiling linings involved in the fire. $\dot{m}_d$ is a vent mixing flow from the upper layer to the lower layer (see section 4.8). In the model, $\dot{m}_d$, $\dot{m}_i$ and $\dot{m}_o$ are provided by the ventflow algorithm (see section 4.9) as a single term representing the net flow to the upper/lower layer due to to all vent flows. $\dot{m}_w$ is a convective wall flow between the layers and may be either positive or negative (see section 4.7). There may also be an additional mass flow term where mechanical ventilation (extract to/from a room from/to an exterior space) is specified (see Section 4.13). This is not shown in the above equations.

4.3 Species Generation

The conservation equation for species in the upper layer is:

$$\frac{dY_{i,u}}{dt} = \frac{1}{M_u}\left[\dot{m}_p(Y_{i,l} - Y_{i,u}) + \dot{m}_f(\Psi_i - Y_{i,u})\right] \tag{4.8}$$

The conservation equation for species in the lower layer is:

$$\frac{dY_{i,l}}{dt} = \frac{1}{M_l}\left[\dot{m}_i(Y_{i,\infty} - Y_{i,l}) + \dot{m}_d(Y_{i,u} - Y_{i,l})\right] \tag{4.9}$$

M_u and M_l are obtained from applying the ideal gas law such that $M_i = MW_i PV_i/(RT_i)$ where i is the upper or lower layer and MW_i is the average molecular weight of the layer based on the gas composition of the layer and R is the universal gas constant.

Species tracked in the model are soot, CO, CO_2, HCN, water vapor, unburned fuel and O_2. The mass fractions of soot, HCN and CO initially present in the room are considered to be negligible, while the initial mass fraction of O_2 is equal to 0.231 (ambient), and of CO_2 equal to 0.0005. Unburned fuel is only 'produced' under a ventilation limited burning regime.

The mass fraction of water vapor, Y_{H2O}, initially present in the room is determined from the known relative humidity and ambient temperature as follows [18]:

$$Y_{H2O} = \frac{0.622\Phi_{\mathrm{RH}}W_s}{W_s + 0.622 - \Phi_{\mathrm{RH}}W_s} \tag{4.10}$$

where Φ_{RH} is the relative humidity, W_s is the humidity ratio at saturation, and 0.622 is the ratio between the molecular weights of water vapor and air. The humidity ratio at saturation [18] is given by:

$$W_s = \frac{0.622 P_{\mathrm{ws}}}{P_a - P_{\mathrm{ws}}} \tag{4.11}$$

where P_{ws} is the saturation pressure for water vapor corresponding to the ambient temperature and is determined from steam tables [19], and P_a is atmospheric pressure.

For a room-corner fire, the species generated by objects/burner, wall linings and ceiling linings are separately accounted for and summed.

4.4 Combustion Chemistry

The user specifies the composition of the fuel by number of atoms of C, H, O and N in a fuel molecule. The molecular weight of the fuel is then calculated using the respective atomic weights as required.

Following the methodology outlined by Ierardi [20], the general combustion equation is given by:

$$C_a H_b O_c N_d + e(O_2 + 3.76 N_2) \rightarrow f CO_2 + g H_2O + h CO + i HCN + j C + k N_2 \tag{4.12}$$

a, b, c, d are knowns. f, h, j are derived from the specified species yields for carbon dioxide, carbon monoxide and soot respectively, such that:

$$n_{product} = \frac{Y_{product} MW_{fuel}}{n_{fuel} MW_{product}} \tag{4.13}$$

For a balanced equation, the following algebraic expressions apply.

$$\begin{aligned} a &= f + h + i + j && (4.14)\\ b &= 2g + i && (4.15)\\ c + 2e &= 2f + g + h && (4.16)\\ d + 7.52e &= i + 2k && (4.17) \end{aligned}$$

Solving the equations simultaneously for the unknowns gives:

$$\begin{aligned} i &= a - f - h - j && (4.18)\\ g &= (b - i)/2 && (4.19)\\ e &= (2f + g + h - c)/2 && (4.20)\\ k &= (d + 7.52e - i)/2 && (4.21) \end{aligned}$$

Therefore, the yield of HCN and H_2O products are:

$$Y_{HCN} = \frac{iMW_{HCN}}{MW_{fuel}} \tag{4.22}$$

$$Y_{H2O} = \frac{gMW_{HCN}}{MW_{fuel}} \tag{4.23}$$

For fires that are underventilated, the yields of CO_2 and H_2O are reduced depending on the calculated plume global equivalence ratio. The global equivalence ratio [21] is calculated as follows:

$$\phi_e = \frac{\Delta H_c \dot{m}_f}{\Delta H_{O2} \dot{m}_p Y_{O2,l}} \tag{4.24}$$

where ΔH_{O2} is taken to be a constant (13.1 MJ/kg).

When the global (plume) equivalence ratio (ger) for the fire compartment is greater than 1 (underventilated fire), the yields are given by:

$$Y_{CO2,vc} = \frac{Y_{CO2,wv}}{\phi} \tag{4.25}$$

$$Y_{H2O,vc} = \frac{Y_{H2O,wv}}{\phi} \tag{4.26}$$

The subscripts *wv* and *vc* are for 'well ventilated' and 'ventilation controlled' respectively. In addition, adjustments are made to the specified fuel heat of combustion and the radiant loss fraction depending on the degree of under-ventilation. Using the correlations provided by Tewarson [22, 23], the heat of combustion and radiant loss fraction are reduced as the global equivalence ratio increases according to:

$$\frac{\Delta H_{ch,vc}}{\Delta H_{ch,wv}} = 1 - \frac{0.97}{\exp((\phi/2.15)^{-1.2})} \tag{4.27}$$

$$\frac{\Delta H_{con,vc}}{\Delta H_{con,wv}} = 1 - \frac{1.0}{\exp((\phi/1.38)^{-2.8})} \tag{4.28}$$

Since the radiant loss fraction is the converse of the convective fraction, rearranging the above equations gives the following expression for radiant loss fraction under ventilation controlled conditions.

$$\lambda_{r,vc} = 1 - \left[\frac{(1 - \lambda_{r,wv}) \left(1 - \frac{1.0}{\exp((\phi/1.38)^{-2.8})}\right)}{\left(1 - \frac{0.97}{\exp((\phi/2.15)^{-1.2})}\right)} \right] \tag{4.29}$$

4.4.1 Soot and Smoke Production

The following correlation for the dependence of the soot yield on the global equivalence ratio was developed by Tewarson, Jiang and Morikawa [22, 23] where $\psi_{s,vc}$ is the soot yield under ventilated controlled conditions, $\psi_{s,wv}$ is the soot yield under well ventilated conditions, ϕ is the global equivalence ratio, and α and ζ are constants dependent on the fuel.

$$\frac{\psi_{s,vc}}{\psi_{s,wv}} = 1 + \frac{\alpha}{\exp(2.5\phi^{-\zeta})} \tag{4.30}$$

4.4.2 Carbon Monoxide Production

The carbon monoxide yield (kg CO per kg fuel mass loss) is calculated using correlations for hexane data by Gottuk [24]. The correlations depend on the global equivalence ratio, ϕ_e, and the upper layer temperature as follows:

For an upper layer temperature ≥ 875 K,

$$\Psi_{CO} = \frac{0.22}{\pi}\tan^{-1}[10(\phi_e - 1.25)] + 0.11 \tag{4.31}$$

For an upper layer temperature < 875 K,

$$\Psi_{CO} = \frac{0.19}{\pi}\tan^{-1}[10(\phi_e - 0.8)] + 0.095 \tag{4.32}$$

where the argument of the tan function is in radians.

The correlations are represented graphically in Figure 4.2.

4.5 Burning Rate Enhancement

The program allows the option of enhancing the burning rate of the fire based on the level of incident radiant flux received at the floor due to heat transfer from the gas layers and the room surfaces. The heat of combustion ΔH_c and heat of gasification of the fuel L_g need to be supplied and an estimate of the surface area of the fuel. If the fuel surface area is entered as zero then the surface area (A) will be calculated as shown in equation 4.33 where $\dot{Q}_f$ is the heat release rate of the free-burning fuel and $\dot{m}''$ is a characteristic burning rate per unit area for the fuel.

$$A = \frac{\dot{Q}_f}{\Delta H_c \dot{m}''} \tag{4.33}$$

The additional heat release from the fuel ΔQ, due to the externally applied radiant heat from the gas layers and the room surfaces $\dot{Q}_e$ is then estimated from equation 4.34 and

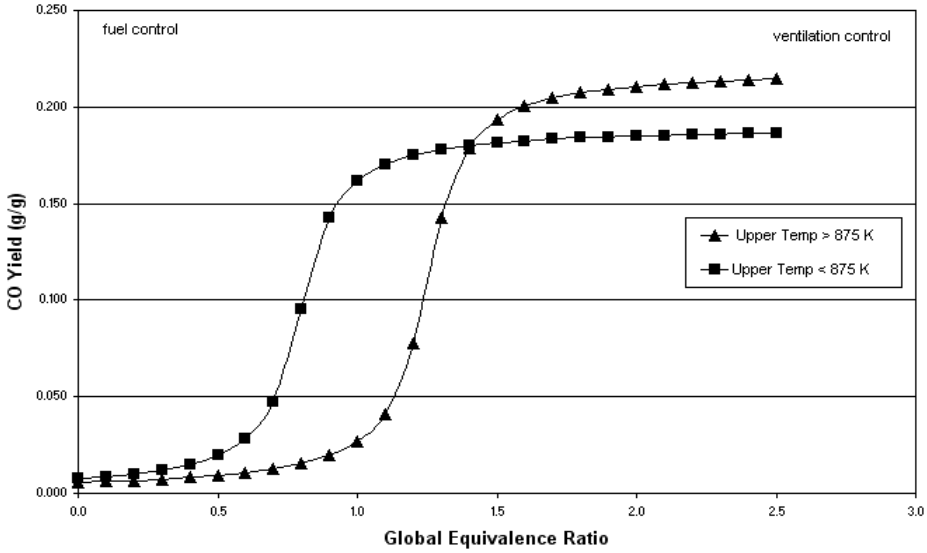

Figure 4.2: Carbon monoxide yields versus global equivalence ratio

this is added to the input (free-burning) heat release rate for use in the energy balance calculations.

$$\Delta Q = A \Delta H_c \frac{\dot{Q}_e}{L_g} \tag{4.34}$$

4.6 Plume Entrainment

Two plume entrainment models are included in *BRANZFIRE* and the user may elect which one to use. The first model is a combination of the strong plume relations and correlations by Delichatsios as presented by Beyler [25], while the second is based on correlations from McCaffrey [26]. McCaffrey's plume correlation is the default.

4.6.1 Strong plume - Delichatsios

The total mass of air entrained into the buoyant plume between the base of the fire and the smoke layer interface depends on the heat release rate and the height as given by Beyler [25] in equations 4.35 and 4.36. In the case of the room-corner fire the plume entrainment is simplified. The total heat release from the burner/source, and that part of the wall lining located below the layer interface height are summed together into a single term, and the plume entrainment is calculated on the basis of a single axi-symmetric plume (modified as described in section 4.6.3) originating from the location of the burner.

$$\dot{m}_p \propto \dot{Q}_c^{1/3} Z^{5/3} \tag{4.35}$$

$$\dot{m}_p = A(1-\lambda_r)^{1/3}\dot{Q}_f^{1/3}Z^{5/3} \tag{4.36}$$

A is an entrainment coefficient correlated with convective heat release. A value of $A = 0.076$ as recommended by Beyler [25] is used. This expression is used when the layer height is above the flame tip, L, given by Heskestad's correlation [8] for fire sources which do not have substantial in-depth combustion.

$$L = -1.02D + 0.23\dot{Q}_f^{2/5} \tag{4.37}$$

When the layer height drops below the height of the flame tip, alternative correlations are used. The correlations are those developed by Delichatsios for a buoyant diffusion flame in the form presented by Beyler [25] as follows:

$$\dot{m}_p = 0.86\left(\frac{Z-Z_o}{D}\right)^{1/2} D^{5/2} \quad \text{for} \quad \frac{Z-Z_o}{D} < 1.0 \tag{4.38}$$

$$\dot{m}_p = 0.93\left(\frac{Z-Z_o}{D}\right)^{3/2} D^{5/2} \quad \text{for} \quad 1.0 < \frac{Z-Z_o}{D} < 5.16 \tag{4.39}$$

$$\dot{m}_p = 0.18\left(\frac{Z-Z_o}{D}\right)^{5/2} D^{5/2} \quad \text{for} \quad 5.16 < \frac{Z-Z_o}{D} < \frac{L}{D} \tag{4.40}$$

The position of the virtual source Z_o is from Heskestad [8].

$$Z_o = -1.02D + 0.083\dot{Q}_f^{2/5} \tag{4.41}$$

For non-circular fire sources, the diameter is calculated on the basis of equivalent area. Since generally only the heat release rate, mass loss rate and effective heat of combustion of the fuel are known, the size (area, diameter) of the fire is estimated assuming a uniform mass loss rate per unit area for the fuel. The diameter of the fire is determined at each timestep from the fuel mass loss rate (derived from the heat release rate and energy yield inputs) and a characteristic value of the mass loss rate per unit area, which may be input or changed by the user.

$$D = \sqrt{\frac{4\dot{m}_f}{\pi\dot{m}_f''}} \tag{4.42}$$

4.6.2 McCaffrey's correlations

The mass flux entrained into the plume for the continuous flaming, intermittent and buoyant plume regions respectively is given by [26]:

$$\dot{m}_p/\dot{Q}_f = 0.011 \left(\frac{Z}{\dot{Q}_f^{2/5}} \right)^{0.566} \quad \text{for} \quad 0 \leq \frac{Z}{\dot{Q}_f^{2/5}} < 0.08 \tag{4.43}$$

$$\dot{m}_p/\dot{Q}_f = 0.026 \left(\frac{Z}{\dot{Q}_f^{2/5}} \right)^{0.909} \quad \text{for} \quad 0.08 \leq \frac{Z}{\dot{Q}_f^{2/5}} < 0.20 \tag{4.44}$$

$$\dot{m}_p/\dot{Q}_f = 0.124 \left(\frac{Z}{\dot{Q}_f^{2/5}} \right)^{1.895} \quad \text{for} \quad 0.20 \leq \frac{Z}{\dot{Q}_f^{2/5}} \tag{4.45}$$

McCaffrey's correlations are empirical, fitted to experimental data and not based on theory. They are however an extension of the common point source plume model with a different set of coefficients for each region [17].

4.6.3 Effect of fire location on plume entrainment

The model allows for burning objects to be located in the centre of the room, against a wall, or in the corner of the room. For these latter cases, the plume entrainment correlations based on the simple Zukowski equation are used [27].

For a corner fire,

$$\dot{m}_p = 0.028 \dot{Q}^{1/3} Z^{5/3} \tag{4.46}$$

For a wall fire,

$$\dot{m}_p = 0.045 \dot{Q}^{1/3} Z^{5/3} \tag{4.47}$$

The entrainment model used here is a simplification of the actual situation. The total heat release from the burner/source, and that part of the wall lining located below the layer interface height are summed together into a single term that is then represented by a fire located at the position and height of the burner.

4.7 Wall Flows

A significant buoyancy-induced flow may arise adjacent to the walls due to convective and radiative heat transfer between the wall surfaces and the heated gas layers. Initially

cooler wall surfaces may induce a downward flow as the hot layer gases are cooled adjacent to the wall. Later as the wall surfaces are heated, there may be an upward flow as lower layer gases are heated. These flows interact and cause mass and energy to be transported between the layers. The flows are distributed in this model according to the relative magnitude of their momentum.

Turbulent and laminar flow regimes are treated differently. The Grashof Number (Gr) is used to define the flow regime with Grashof Number $> 5 \times 10^{-9}$ for turbulent flow and Grashof Number $< 5 \times 10^{-9}$ for laminar flow.

$$Gr = g\beta\Delta T Z^3/\nu^2 \tag{4.48}$$

$g = 9.81$, $\beta = 1/T$, ΔT is the temperature difference betwen the wall surface and the adjacent gas layer and ν is the kinematic viscosity of the gases $\nu = 7.18 * 10^{-10}((T_g + T_s)/2)^{7/4}$. Z is taken as the applicable layer depth. ρ is the density of the gas layer and Prandtl Number (Pr) = 0.69. P is the horizontal wall perimeter of the room excluding opening widths.

The buoyancy-induced mass flow adjacent to the wall for turbulent conditions is:

$$\dot{m}_w = 0.1463 P\rho\delta U \tag{4.49}$$

$$\delta = 0.565(Gr)^{-1/10} Pr^{-8/15}[1 + 0.494(Pr)^{2/3}]^{1/10} \tag{4.50}$$

$$U = 1.185\frac{\nu}{Z}(Gr)^{1/2}[1 + 0.494(Pr)^{2/3}]^{-1/2} \tag{4.51}$$

The buoyancy-induced mass flow adjacent to the wall for laminar conditions is:

$$\dot{m}_w = P\rho\delta U/12 \tag{4.52}$$

$$\delta = 3.93 Pr^{-1/2}\left(Pr + \frac{20}{21}\right)^{1/4}\left(\frac{g\beta\Delta T}{\nu^2}\right)^{-1/4} Z^{1/4} \tag{4.53}$$

$$U = 5.17\nu\left(Pr + \frac{20}{21}\right)^{-1/2}\left(\frac{g\beta\Delta T}{\nu^2}\right)^{1/2} Z^{1/2} \tag{4.54}$$

At any particular time, the existence and magnitude of any wall flow from the upper to lower layer (for $T_u > T_{s,u}$), and from the lower to upper layer (for $T_l < T_{s,l}$) is determined. These two flows are combined and then re-distributed between the two gas layers depending on the relative momentum of each of the flows.

The flow momentum is given by:

$$\dot{M}_w = P\rho\delta U^2/105 \text{ for laminar flow} \tag{4.55}$$

$$\dot{M}_w = 0.0523 P \rho \delta U^2 \text{ for turbulent flow} \tag{4.56}$$

The flow deposited in the lower layer is then determined as:

$$\dot{m} = (\dot{m}_{w,u} + \dot{m}_{w,l}) \times \frac{\dot{M}_{w,u}}{\dot{M}_{w,l} + \dot{M}_{w,u}} \tag{4.57}$$

The flow deposited in the upper layer is:

$$\dot{m} = (\dot{m}_{w,u} + \dot{m}_{w,l}) \times \left(1 - \frac{\dot{M}_{w,u}}{\dot{M}_{w,l} + \dot{M}_{w,u}}\right) \tag{4.58}$$

4.8 Vent Mixing

When cool air flows into the room, it is assumed to entrain some of the upper layer gases from the upper layer into the lower layer. This shear entrainment is based on a correlation by Quintiere and McCaffrey [28] as follows:

$$\dot{m}_d = k \left(\frac{T_{\text{l,in}}}{T_u}\right) \left(1 - \frac{Z}{Z_n}\right) \left(\frac{w}{w_o}\right)^n \dot{m}_i \tag{4.59}$$

where: $k = 0.5$, an empirical factor and $n = 0.25$ as suggested by Quintiere and McCaffrey [28]. Z_n is the height of the neutral pressure plane and Z is the layer height. w_o is the vent width, and w is the width to which the outward vent flow expands and is taken as the relevant dimension nominated by the user in the vent-geometry screen where the inflow is from another room and four times the vent width when the inflow is from the outside. This vent mixing flow from upper to lower layer applies both to vents to the exterior and vents to adjacent rooms.

In the case of vents connecting two rooms there is a mixing phenonemon which occurs, where the mass flow out through the vent causes additional air from the lower layer of the adjacent room to be entrained and deposited in the upper layer of the adjacent room. This entrainment flow is assumed to only occur when the layer height in the source room is lower than the layer height in the destination room. The flow is determined using equations given by Peacock et al [17] for the CFAST model.

4.9 Vent Flows

4.9.1 Natural vent flow through walls

The mass flow of air and hot gases through a wall vent is driven by buoyancy. Bernoulli's equation can be used to calculate the flows. Derivation and discussion of buoyancy-driven vent flow equations can be found in many places in the literature [29, 30, 31, 32, 33].

BRANZFIRE uses natural ventflow routines developed by Cooper and Forney [34] from a computer code application known as CCFM.VENTS. A complete description of the physical basis can be found in the literature [34, 35, 36, 37], and only a brief description will be included here.

The vent flow calculations are the result of room to room cross-vent hydrostatic pressure differences. Only rectangular vents in walls are currently considered.

At each point in time, the vent flow calculation is carried out in three stages. Firstly, the hydrostatic pressure profile over the height of a common wall including a vent is determined. The pressure difference across the vent will drive the room to room vent flow. The second stage determines the characteristics of each individual vent, which may involve from one to six horizontal slabs of uniform property, uni-directional flow. The third stage keeps track of the source and destination of each of these slab flows. CCFM.VENTS includes rules for distributing the vent flow into an adjacent room (upper or lower layer) depending on the relative temperatures of the layers and flow. The temperature of the vent flow is required to be at least 3 K above the temperature in the adjacent room before an upper layer will start to form.

Vents can be opened and closed during the simulation at the time nominated by the user. This opening/closing is not instantaneous but is assumed to occur over a two second period by a linear increase in the width of the vent from fully closed to fully open (and vice versa).

4.9.2 Natural vent flow through ceilings and floors

The vent flow algorithm VENTCF2A [38] is used for modelling the gas flows through a ceiling or floor vent. The vent may connect to the outside, or it may connect to another room. The flow is driven by cross-vent pressure differences and, when appropriate, combined pressure and buoyancy-driven flows which occur when the density configuration is unstable. This occurs when a dense cooler gas layer is above the vent and a less dense hot gas layer is directly below the vent. For unstable density configurations, VENTCF2A is for flow through a circular, shallow (small ratio of depth-to-diameter) horizontal vent. It is expected that it can be used for non-circular vents provided the aspect ratio is not too different from unity [38].

Vents can be opened and closed during the simulation at the time nominated by the user. This opening/closing is not instantaneous but is assumed to occur over a two second period by a linear increase in the area of the vent from fully closed to fully open (and vice versa). Vents can also be automatically opened by the activation of a thermal or smoke detector located within the room immediately below the vent.

These vent flow routines are applicable where the vent area is small compared to the ceiling area. They should not be used to model large openings in floors to accommodate atria etc. In such cases it is better to model a void as a separate space connected to adjacent rooms with wall vents.

4.10 Oxygen Limited Burning

The model takes into account the available air supply and its effect on the heat release rate. The approach taken is to determine the mass flow of oxygen in the plume and compare it to the amount needed for complete combustion of the fuel. If the flow is found to be insufficient, combustion may still be completed by oxygen present in the upper layer, but only if the upper layer oxygen concentration is greater than a critical value. The relevant equations are as follows.

4.10.1 Mass flow of oxygen needed for complete combustion

The mass flow of oxygen in the plume (kg-O_2/sec) needed for complete combustion of the fuel is given by:

$$\dot{m}_{\text{oxygen needed}} = \frac{\dot{Q}_f}{13100} \tag{4.60}$$

This equation is based on the observation that approximately 13100 kJ of energy is released for every kg of oxygen consumed during the combustion reaction [39].

4.10.2 Mass flow of oxygen present in the plume

The actual mass flow of oxygen in the plume (kg-O_2/sec) is given by:

$$\dot{m}_{\text{oxygen actual}} = \dot{m}_p Y_{O_2,L} \times C \tag{4.61}$$

where C is a coefficient described by Peacock et al [17] representing the fraction of fuel that can be burned with the available oxygen and varies between 0 and 1 to provide a smooth cut-off of the burning over a narrow range above the oxygen limit. An oxygen limit of 10% by volume is assumed.

$$C = \frac{\tanh(800(Y_{O_2,L} - Y_{\text{limit}}) - 4) + 1}{2} \tag{4.62}$$

$$Y_{\text{limit}} = \frac{\text{Molecular Weight } O_2}{\text{avg Molecular Weight of lower layer}} \times 0.1 \tag{4.63}$$

4.10.3 Oxygen concentration in the upper layer

The oxygen concentration in the upper layer is given by:

$$\%\ \text{Vol } O_2 = Y_{O_2} \times \frac{\text{avg Molecular Weight of Upper Layer}}{\text{Molecular Weight of } O_2} \times 100 \tag{4.64}$$

The average molecular weight of the upper layer is determined from the mass fractions of oxygen, carbon dioxide, carbon monoxide and water vapour with the balance of the layer assumed to be nitrogen as follows.

$$MW_{\text{avg}} = Y_{O_2} MW_{O_2} + Y_{CO_2} MW_{CO_2} + Y_{CO} MW_{CO} + Y_{H_2O} MW_{H_2O} + Y_{N_2} MW_{N_2} \quad (4.65)$$

4.10.4 Minimum oxygen concentration needed for combustion

The minimum oxygen concentration needed for combustion to occur is assumed to vary between 2 and 10% depending on the gas temperature. The method for determining the limiting value is the same as that used in FPETool [40] and is given by:

$$\%\ \text{Vol O}_2\ \text{critical} = \frac{T_{\text{fo}} - T_u}{T_{\text{fo}} - T_\infty}[O_{\text{L1}} - O_{\text{L2}}] + O_{\text{L2}} \quad (4.66)$$

Where T_{fo} is a designated flashover temperature (873 K), T_u is the upper layer temperature (K), T_∞ is the ambient temperature (in K), O_{L1} is the minimum oxygen concentration required for combustion near room temperature (10%), and O_{L2} is the minimum oxygen concentration required for combustion near flashover temperatures (2%).

4.11 Postflashover Model

An optional postflashover model can be selected. Flashover is defined as when the radiation heat flux on the floor exceeds 20 kW/m^2. To use this model, the fire object initially used must have sufficient intensity to generate a heat flux of this level on the floor. Initially the preflashover model is used based on the heat release and other characteristics of the selected fire object. However, following the attainment of 'flashover' a switch to the postflashover model occurs. The model keeps track of the total amount of fuel consumed during the simulation, and when all the fuel is consumed the mass loss rate is set equal to zero.

The postflashover model, based on Babrauskas' COMPF2 model [33], requires determination of a ventilation-controlled mass loss rate, a fuel surface area controlled mass loss rate and a crib porosity controlled mass loss rate, with the lesser of the three rates governing the pyrolysis rate. The postflashover model assumes behaviour representative of wood cribs and additional input parameters are required to be specified. They are:

- an average heat of combustion representative of the total combustible fuel load in the room
- an average fuel density
- the fire load energy density per unit floor area

- a characteristic stick thickness (d)
- stick spacing (s)

4.11.1 Postflashover mass loss rate

The mass loss rate for ventilation controlled burning rate is given by the following. Only vent openings connected to the outside (and not to interior rooms) are utilised in this calculation, with $A\sqrt{h}$ summed for multiple vents.

$$\dot{m}_f = 0.12A\sqrt{h} \tag{4.67}$$

The fuel surface area controlled mass loss rate is:

$$\dot{m}_f = \frac{4}{d} m_o v_p \sqrt{\frac{m}{m_o}} \tag{4.68}$$

v_p is a surface regression rate for wood and taken as $0.0000022d^{-0.6}$. m is the mass of fuel remaining, and m_o is the original mass of fuel (determined using the specified floor area and fuel load energy per unit floor area).

The crib porosity controlled mass loss rate is:

$$\dot{m}_f = 0.44 \frac{s}{\Delta H_c} \frac{m_o}{d} \tag{4.69}$$

The governing mass loss rate (lesser of the three) is multiplied by the average heat of combustion to give the rate of heat release used in the zone model conservation equations.

4.11.2 Postflashover plume entrainment

When flashover is deemed to have occurred a large simplification is necessary for the calculation of plume entrainment, as the pre-flashover models are no longer strictly valid. After flashover, the plume entrainment is calculated using the McCaffrey 'flaming' correlation as follows. $\dot{Q}_{max}$ is the maximum heat release that can be supported by the available oxygen supply.

$$\dot{m}_p / \dot{Q}_{max} = 0.011 \left(\frac{Z}{\dot{Q}_{max}^{2/5}} \right)^{0.566} \tag{4.70}$$

4.12 Glass Fracture Model

An automatic glass fracture model is included based on work by Parry [41, 42]. The model is largely based on the heat transfer model developed by Sincaglia and Barnett [43]

and the fracture criterion of Pagni and Joshi [44]. The finite difference scheme stability criterion was revised from that presented by Sincaglia and Barnett. Routines for assessing flame flux heating have been added. Parry reported that BRANZFIRE predicted a fracture time consistent with experimental results from Skelly, Roby and Beyler [45].

Readers are referred to the publications by Parry [41, 42] for details of how the model has been implemented within BRANZFIRE.

4.13 Mechanical Ventilation

Mechanical ventilation by supplying or exhausting gases from specified rooms is permitted. Multiple fans per room are permitted but they each must be located at the same height and have the same flow rate specification. The implementation is by adding (pressurisation) or removing (extraction) a specified flow rate (m^3/s converted to kg/s) from the layer in which the fan is located (as determined by the specified elevation height of the fan) and including this flow in the mass and energy balance equations described earlier. A fan straddling the layer interface is not considered, the fan is assumed to be either totally within the upper or lower layer. Optionally, the use of a fan curve can be selected. If this is not done, the program will extract/supply air to the space at the flow rate specified, irrespective of the cross-fan pressure differences. If the fan curve option is selected, the actual flow rate equals the specified flow rate when the cross-fan pressure difference is zero, and monotonically reduces to zero as the cross-fan pressure difference reaches the specified pressure limit as described in equations 4.71 and 4.72, where $\dot{V}'$ is the actual flow rate through the fan, $\dot{V}$ is the specified flow rate through the fan, ΔP_L is the specified maximum pressure across the fan, and ΔP_{cf} is the actual cross-fan pressure difference.

$$\dot{V}' = \dot{V}\left[\frac{\Delta P_L - \Delta P_{cf}}{\Delta P_L}\right]^{1/6} \quad \text{for } \Delta P_L > \Delta P_{cf} \tag{4.71}$$

$$\dot{V}' = -\dot{V}\left[\frac{\Delta P_{cf} - \Delta P_L}{\Delta P_L}\right]^{1/6} \quad \text{for } \Delta P_L < \Delta P_{cf} \tag{4.72}$$

The user specifies the activation time of the fan, and the flow rate is assumed to linearly increase from zero to the design flow rate over a period of 30 seconds representing a fan start-up delay. Alternatively the fan can be automatically started following the actuation of a smoke detector in the same room.

Figure 4.3 shows a generic fan curve for a user specified extract rate of 100 m^3/s and a cross-fan pressure limit of 50 Pa.

The phenomenon of 'plugholing' is incorporated into the calculations. This occurs when the layer is thin and both upper and lower layer gases are drawn through the fan, instead of from only the gas layer immediately surrounding the fan.

The maximum mass flow rate through the fan before plugholing occurs is calculated [46].

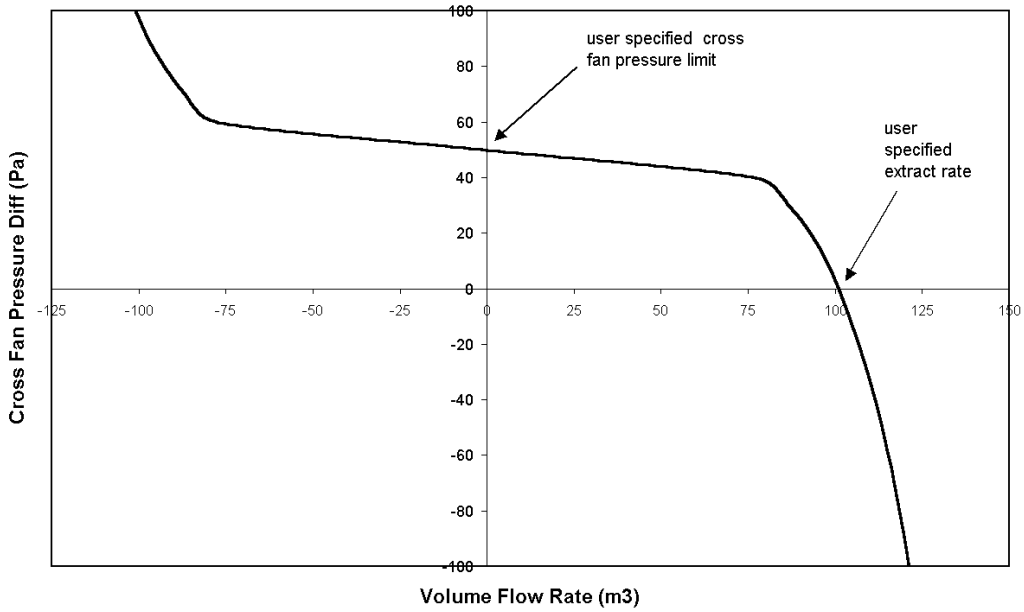

Figure 4.3: A generic fan curve

$$M_{crit} = 1.6\rho_u(H-z)^{5/2}\sqrt{1-\frac{\rho_u}{\rho_l}} \tag{4.73}$$

In the event that the specified mass flow through the fan exceeds this critical value, M_{crit} is taken from the upper layer and the balance is taken from the lower layer.

4.14 Vent Fires

In the event of ventilated-limited burning conditions, there will be insufficient oxygen for complete combustion of the fuel, and therefore it is necessary to account for mass flows of unburned fuel. When the mass flow passes through a vent (to the outside or into another room) it may mix with oxygen and burn in the form of a vent fire, releasing combustion energy into the adjacent space or to the outside.

The criteria used for external burning i.e vent fires is taken from Beyler [47] where the equivalence ratio at which layer burning begins is:

$$\phi_{ig} = \frac{k}{k-r-1} = \frac{k}{k-\Delta H_{air}/\Delta H_c - 1} \tag{4.74}$$

where

$$k = \frac{\Delta H_{O2} Y_{O2}}{c_p T_{ad} - T_o} \tag{4.75}$$

$\Delta H_{O2} = 13.4$ MJ/kg. Y_{O2} is the mass fraction of oxygen in the lower layer of the destination room. $T_{ad} = 1700$ K, is the adiabatic flame temperature of the stoichiometric mixture, T_o is the precombustion temperature resulting from stoichiometric mixing of the air and fuel streams, where the upper layer of the fire room contains the fuel stream and the lower layer of the destination room contains the air stream.

$$T_o = \frac{T_u + (Y_f/r)T_l}{1 + Y_f/r} \tag{4.76}$$

4.15 Heat Transfer

4.15.1 Radiation exchange model

The model incorporates a four wall radiation exchange algorithm following the method described by Forney [48]. This algorithm allows the ceiling, upper wall, lower wall and floor to transfer radiation independently between each other. Radiant heating of these surfaces by the flames is also considered by treating the fire as a point source. The emission of radiation by soot particles in the upper layer and absorption by carbon dioxide and water vapor is also considered for both layers. The upper wall comprises those parts of the wall above the height of the smoke layer interface, while the lower wall comprises those parts below the interface.

The radiation exchange submodel is required to determine the net radiant heat flux emitted or absorbed by each room surface (i.e. upper and lower walls, ceiling and floor). These radiant fluxes are combined with the convective heat flux and used as the boundary condition for the heat conduction calculations described later. The gas layer absorption due to carbon dioxide and water vapor, and emission due to soot particles are required for the energy source terms in the ordinary differential equations of the zone model.

Assumptions

The following assumptions are made in developing the four wall radiation exchange model [48].

1. Both gas layers and each of the wall, ceiling and floor surfaces are assumed to be at a uniform temperature. This is generally not true where the surfaces meet each other.

2. The surfaces and gas layers are assumed to be in quasi-steady state, remaining constant over the duration of the time step of the associated differential equations.

3. For the purposes of estimating the radiation heat transfer from the flame, the total fire is assumed to radiate uniformly in all directions from a single point source.

4. The radiation emitted by the room surfaces, gas layers and the fire is assumed to be diffuse and gray (i.e. the radiant flux is assumed independent of direction and wavelength).

5. The room surfaces are assumed to be opaque (i.e. incident radiation is either reflected or absorbed not transmitted) and the gases are assumed to be non-reflective.

6. The room is assumed to be a rectangular box with each surface either perpendicular or parallel to every other surface. Radiation losses through room openings are included.

Heat flux striking a surface

Heat flux striking a room surface may be due to radiation from the flames assuming a point source fire, or it may be due to the radiating upper or lower gas layers, or it may be due to radiation from other room surfaces. If the gas layers are transparent then the heat flux striking the k^{th} surface due to the fire is given by Forney [48] as:

$$q''_{f-k} = \frac{\lambda_r \dot{Q}_f \omega_{f-k}}{4\pi A_k} \tag{4.77}$$

The fraction of the radiant energy leaving the f^{th} fire and intercepted by the k^{th} surface is given by $\omega_{f-k}/(4\pi A_k)$ and is a configuration factor. ω_{f-k} is the solid angle between the point source fire and the k^{th} surface. Other symbols are as given in the nomenclature.

If the gas layers are not transparent then there are four cases depending on whether the fire is located in the upper or lower layer. In this model, to simplify the situation, the fire will be assumed to be located in the lower layer.

The heat flux striking the k^{th} room surface due to an emitting i^{th} gas layer is given as:

$$q''^{\text{i,gas}}_{j-k} = \alpha^i_{j-k} \sigma T_i^4 \tag{4.78}$$

where $\alpha^i_{j-k} = 1 - \tau^i_{j-k}$, α^i_{j-k} is the absorptivity of the gas and τ^i_{j-k} is the transmissivity of the gas.

Table 4.1 is taken from Forney [48] [1] and summarises the radiative flux striking the k^{th} room surface due to a point source fire and an emitting gas layer.

Solid angles

The fraction of the radiant heat flux from a point source which is intercepted by a wall surface is found using solid angles as described by Forney [48]. For a surface with sides of dimensions x and y, and in a plane a distance r from the radiating point source, the solid angle is:

[1] differs slightly - some of the entries in columns 3 and 4 above are transposed in the original.

Table 4.1: Radiative heat flux striking the k^{th} room surface

Path	**Fire**	**Gas Layer**	
	q''^{fire}_{f-k}	$q''^{\text{L,gas}}_{j-k}$	$q''^{\text{U,gas}}_{j-k}$
upper to upper	$\tau^U_{f-k}\frac{\lambda_r \dot{Q}_f \omega_{f-k}}{4\pi A_k}$	0	$F_{k-j}\sigma\alpha^U_{j-k}T^4_u$
lower to upper	$\tau^U_{f-k}\tau^l_{f-k}\frac{\lambda_r \dot{Q}_f \omega_{f-k}}{4\pi A_k}$	$F_{k-j}\sigma\alpha^L_{j-k}T^4_l$	$F_{k-j}\sigma\alpha^U_{j-k}T^4_u\tau^L_{j-k}$
upper to lower	$\tau^L_{f-k}\tau^U_{f-k}\frac{\lambda_r \dot{Q}_f \omega_{f-k}}{4\pi A_k}$	$F_{k-j}\sigma\alpha^L_{j-k}T^4_l\tau^L_{j-k}$	$F_{k-j}\sigma\alpha^U_{j-k}T^4_U$
lower to lower	$\tau^L_{f-k}\frac{\lambda_r \dot{Q}_f \omega_{f-k}}{4\pi A_k}$	$F_{k-j}\sigma\alpha^L_{j-k}T^4_l$	0

$$\omega(x,y) = \frac{1}{4\pi}\left\{\sin^{-1}\left(A\frac{y}{\sqrt{y^2+r^2}}\right) + \sin^{-1}\left(A\frac{x}{\sqrt{x^2+r^2}}\right) - \frac{\pi}{2}\right\} \tag{4.79}$$

$$\text{where } A = \sqrt{1+\frac{r^2}{x^2+y^2}}$$

Solid angles for each of the various surfaces are additive with the relevant geometry shown in Figure 4.4.

Configuration factors

There are a total of 16 configuration factors between the four surfaces to be considered in the room. For the purposes of this section the four room surfaces will be labelled 1 to 4 as shown in Figure 4.5. The layer interface is considered to be a "pseudo-surface" labelled "d".

The configuration factors to be determined are as follows:

$$F_{i-j} \text{ for } i,j = 1,...,4. \tag{4.80}$$

All the configuration factors can be determined in terms of F_{1-4}, F_{1-d} and F_{4-d}.

F_{1-4} does not change during the simulation and thus neeed only be calculated once for the room. It may be determined from the configuration factor between two parallel rectangular plates, at a distance L apart, as given by Incropera and deWitt [49].

$$\begin{aligned} F_{1-4} &= \frac{2}{\pi\overline{X}\overline{Y}}\left\{\ln\left[\frac{(1+\overline{X})^2(1+\overline{Y})^2}{1+\overline{X}^2+\overline{Y}^2}\right]^{1/2} + \overline{X}\sqrt{1+\overline{Y}^2}\tan^{-1}\left(\frac{\overline{X}}{\sqrt{1+\overline{Y}^2}}\right)\right. \\ &+ \left.\overline{Y}\sqrt{1+\overline{X}^2}\tan^{-1}\left(\frac{\overline{Y}}{\sqrt{1+\overline{X}^2}}\right) - \overline{X}\tan^{-1}\overline{X} - \overline{Y}\tan^{-1}\overline{Y}\right\} \end{aligned} \tag{4.81}$$

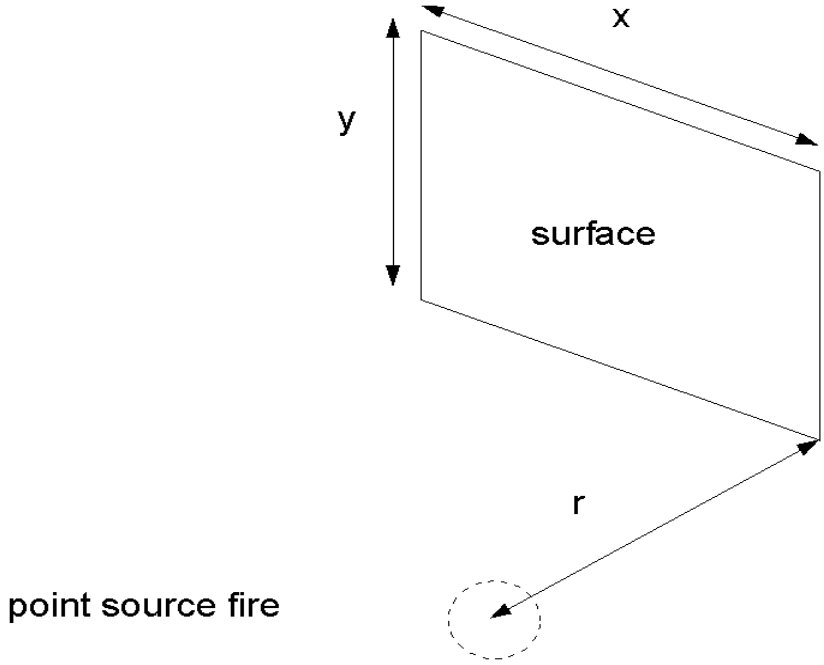

Figure 4.4: Geometry for determination of solid angles

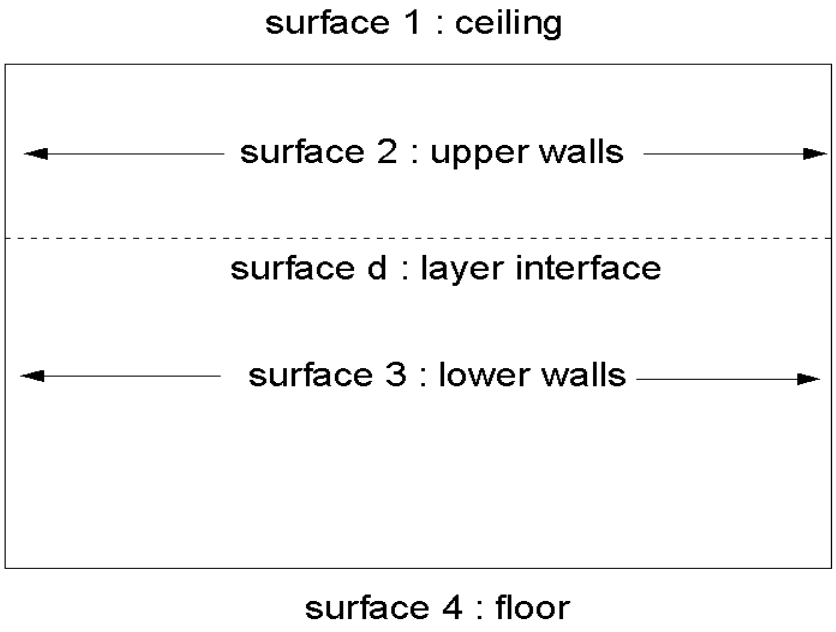

Figure 4.5: Schematic showing the surfaces considered in the configuration factor formulae

where $\overline{X} = X/L$ and $\overline{Y} = Y/L$ and X and Y are the length and width of the rectangles respectively.

F_{1-d} and F_{4-d} can be calculated in the same way using equation 4.81, but since the position of the smoke layer interface changes during the fire simulation, they need to be calculated at each time step.

From the reciprocity theorem, $F_{1-4} = F_{4-1}$ since the floor and ceiling areas are assumed to be equal, and the remaining 14 configuration factors can now be determined using simple algebraic formulae by making use of the following configuration factor properties.

$$A_j F_{j-k} = A_k F_{k-j} \tag{4.82}$$

$$F_{i,j\oplus k} = F_{i-j} + F_{i-k} \tag{4.83}$$

$$A_{i\oplus j} F_{i\oplus j-k} = A_i F_{i-k} + A_j F_{j-k} \tag{4.84}$$

$$\sum_{k=1}^{N} F_{j-k} = 1,\ j = 1, ..., N \tag{4.85}$$

where $i \oplus j$ denote the union of two surfaces i and j.

The floor and ceiling are assumed to be flat rectangular surfaces so that

$$F_{1-1} = F_{4-4} = 0 \tag{4.86}$$

Since the sum of the configuration factors in an enclosure is 1, and symmetry results in $F_{2-1} = F_{2-d}$, it follows that:

$$\begin{aligned} F_{1-2} + F_{1-d} &= 1 \\ F_{2-1} + F_{2-2} + F_{2-d} &= 2F_{2-1} + F_{2-2} = 1 \end{aligned}$$

It therefore follows that:

$$\begin{aligned} F_{1-2} &= 1 - F_{1-d} \\ F_{2-1} &= \frac{A_1}{A_2} F_{1-2} \\ F_{2-2} &= 1 - 2F_{2-1} \\ F_{4-3} &= 1 - F_{4-d} \\ F_{3-4} &= \frac{A_4}{A_3} F_{4-3} \\ F_{3-3} &= 1 - 2F_{3-4} \\ F_{1-3} &= 1 - F_{1-4} \\ F_{3-1} &= \frac{A_1}{A_3} F_{1-3} \end{aligned}$$

$$
\begin{aligned}
F_{3-2} &= 1 - F_{3-1} - F_{3-3} - F_{3-4} \\
F_{2-3} &= \frac{A_3}{A_2} F_{3-2} \\
F_{2-4} &= 1 - F_{2-1} - F_{2-2} - F_{2-3} \\
F_{4-2} &= \frac{A_2}{A_4} F_{2-4}
\end{aligned}
$$

Transmission factors

The transmission factor is the fraction of energy which passes unimpeded through the gas. It depends on the absorption coefficient of the soot, and on the path length travelled through the gas. The transmission factor is given by:

$$\tau_t = 1 - \alpha_t = 1 - \epsilon_t \tag{4.87}$$

Where α is the total absorptance and ϵ_t is the total emissivity of the gas-soot mixture.

The emissivity of a gas-soot mixture is given by Tien et al [50] as:

$$\epsilon_t = (1 - e^{-k_s L}) + \epsilon_g e^{-k_s L} \tag{4.88}$$

where ϵ_g is the emissivity of the gas alone, and k_s is the effective absorption coefficient of the soot. The absorption coefficient is approximated using the extinction coefficient for the layer (and neglecting the scattering coefficient), calculated from equation 4.115 based on the concentration of the soot in the gas layer and the particle extinction cross-section.

The mean path length, L, is determined from an expression for an arbitrarily shaped gas volume given by Tien et al [50] as follows:

$$L \approx C L_o \tag{4.89}$$

$$\text{where } L_o = \frac{4V}{A} \tag{4.90}$$

Where V and A are the volume and area of the boundary surface of the gas body (upper or lower layer) respectively, and C is a correction factor equal to 0.9 for arbitrary volumes.

The emissivity of the gas is strongly dependent on absorption by water vapor and carbon dioxide over certain wavelength bands. The emissivity of water vapor and carbon dioxide can be determined from charts if the partial pressure and temperature of each gas is known in addition to the mean beam length. Emissivity data [49] for these two gas constituents is incorporated into the model.

The partial pressures are determined from the known mass fractions using the ideal gas law as follows:

$$p_i = \frac{m_i RT}{MW_i V} = \frac{Y_i MRT}{MW_i V} = \frac{Y_i R \rho T}{MW_i} \tag{4.91}$$

$$\Rightarrow p_i = \frac{Y_i R \rho_\infty T_\infty}{MW_i} \tag{4.92}$$

Where p_i is the partial pressure of species i, m_i is the mass of species i, R is the universal gas constant, MW_i is the molecular weight of species i, T and V are the temperature and volume of the gas/air layer, and ρ_∞ and T_∞ are the reference density and temperature for air.

The mass fractions for the water vapor and carbon dioxide are solved for in the ODE equations based on the equations given in Section 4.3.

Solving the net radiation equations

Net radiation refers to the difference between the radiation which is incident on the surface and that which is emitted by the surface. Incoming radiation consists of gray-body surface radiation from the other surfaces, from the radiating fire source, and from the upper and lower gas layers. Outgoing radiation consists of gray-body surface radiation and incoming radiation that has been reflected. Forney [48] gives the net radiation equation to be solved as:

$$\Delta\hat{q}''_k - \sum_{j=1}^{N}(1-\epsilon_j)\Delta\hat{q}''_j F_{k-j}\tau_{j-k} = \sigma T_k^4 - \sum_{j=1}^{N}\sigma T_j^4 F_{k-j}\tau_{j-k} - \frac{c_k}{A_k} \tag{4.93}$$

The matrix corresponding to this linear set of equations is diagonally dominant and therefore may be solved more easily by iterative methods. Ultimately the matrix holding the net radiation leaving each surface, $\Delta q''_k$ is required where $k = 1, ..., 4$. This is related to $\Delta\hat{q}''_k$ by the following expression.

$$\Delta q''_k = D\Delta\hat{q}''_k \tag{4.94}$$

where matrix D is a scaling matrix holding the emittances of the k^{th} room surface elements as follows:

$$D = \begin{pmatrix} \epsilon_1 & 0 & 0 \\ 0 & \ddots & 0 \\ 0 & 0 & \epsilon_N \end{pmatrix} \tag{4.95}$$

The equation to be solved in matrix form is:

$$\hat{A}\Delta\hat{q}''_k = Aq''_k = BE - c''_k \tag{4.96}$$

$$\text{where } c''_k = \frac{c_k}{A_k} = \sum_{j=1}^{N}(q''^{U,gas}_{j-k} + q''^{L,gas}_{j-k}) + \sum_{f=1}^{N^{\text{fire}}} q''^{\text{fire}}_{f-k} \tag{4.97}$$

$q''^{U,gas}_{j-k}$ and $q''^{L,gas}_{j-k}$ account for the radiative flux striking the k^{th} surface due to the upper and lower gas layers respectively, and q''^{fire}_{f-k} accounts for the radiative flux striking the k^{th} surface due to a point source fire.

Matrix E is a column vector with the k$^{\text{th}}$ component as follows.

$$E_k = \sigma T_k^4 \tag{4.98}$$

The k^{th} and j^{th} components of the $N \times N$ matrix B is:

$$b_{k,j} = \delta_{k,j} - F_{k-j}\tau_{j-k} \tag{4.99}$$

where $\delta_{k,j}$ is the Kronecker delta function. The components of the $N \times N$ matrix $\hat{A}$ are as follows:

$$\hat{a}_{k,j} = a_{k,j}\epsilon_j = \delta_{k,j} - F_{k-j}\tau_{j-k}(1-\epsilon_j) \tag{4.100}$$

Equation 4.96 is solved using a LU decomposition technique [51]. The matrix $\hat{A}$ is first decomposed according to the LU algorithm. Then, back substitution of the decomposed matrix results in the solution vector. Once the column vector $\hat{q}''_k$ is found, q''_k which holds the net radiant heat fluxes for the four room surfaces, can then be found from equation 4.94. The model output provides a value for "target radiation". This corresponds to the net incident radiation on the surface of the floor.

Energy absorbed by the gas layers

The energy absorbed by a gas layer may be due to radiation from the point source fires, radiation from the surrounding room surfaces, or from emission from the other gas layer. The net radiant heat absorbed by the upper and lower layers for the different paths are shown in Tables 4.2 and 4.3 taken from Forney [48].

Table 4.2: Radiant heat absorbed by the upper layer

Path through the gas	**Due to heat emitting surface** $q^{\text{out}}_{j-k} = A_j F_{j-k}\left(\sigma T_j^4 - \frac{1-\epsilon_j}{\epsilon_j}\Delta q''_j\right)$	**Due to gas layer emission** $q^{\text{i,gas}}_{j-k} = \alpha^i_{j-k}\sigma T_i^4 A_j F_{j-k}$	**Due to point source fire** $q''^{\text{fire}}_{f-k} = \frac{\lambda_r \dot{Q}_f \omega_{f-k}}{4\pi A_k}$
upper to lower or upper	$q^{\text{out}}_{j-k}\alpha^U_{j-k}$	$-q^{\text{U,gas}}_{j-k}$	$q''^{\text{fire}}_{f-k}\alpha^U_{f-k}A_k$
lower to upper	$q^{\text{out}}_{j-k}\tau^L_{j-k}\alpha^U_{j-k}$	$q^{\text{L,gas}}_{j-k}\alpha^U_{j-k} - q^{\text{U,gas}}_{j-k}$	$q''^{\text{fire}}_{f-k}\alpha^U_{f-k}\tau^L_{f-k}A_k$
lower to lower	0	0	0

Table 4.3: Radiant heat absorbed by the lower layer

Path through the gas	**Due to heat emitting surface** $q_{j-k}^{\text{out}} = A_j F_{j-k}\left(\sigma T_j^4 - \frac{1-\epsilon_j}{\epsilon_j}\Delta q_j''\right)$	**Due to gas layer emission** $q_{j-k}^{\text{i,gas}} = \alpha_{j-k}^{i}\sigma T_i^4 A_j F_{j-k}$	**Due to point source fire** $q_{f-k}''^{\text{fire}} = \frac{\lambda_r \dot{Q}_f \omega_{f-k}}{4\pi A_k}$
lower to lower or upper	$q_{j-k}^{\text{out}}\alpha_{j-k}^{L}$	$-q_{j-k}^{\text{L,gas}}$	$q_{f-k}''^{\text{fire}}\alpha_{f-k}^{L}A_k$
upper to lower	$q_{j-k}^{\text{out}}\tau_{j-k}^{U}\alpha_{j-k}^{L}$	$q_{j-k}^{\text{U,gas}}\alpha_{j-k}^{L} - q_{j-k}^{\text{L,gas}}$	$q_{f-k}''^{\text{fire}}\alpha_{f-k}^{L}\tau_{f-k}^{U}A_k$
upper to upper	0	0	0

Radiation Losses Through Openings

Heat may be lost from the compartment due to radiation through the room openings. It is assumed that the radiation is always lost to the outside, even if the opening is in fact to another compartment. The radiation loss reduces the enthalpy of the upper or lower layer as shown below, where $A_{v,u}$ and $A_{v,l}$ are the vent areas located in the upper and lower gas layers respectively.

$$\dot{q}_{\text{rad,u}} = -\epsilon_{\text{g,u}}\sigma(T_u^4 - T_\infty^4)A_{v,u} \tag{4.101}$$

$$\dot{q}_{\text{rad,l}} = -\epsilon_{\text{g,l}}\sigma(T_l^4 - T_\infty^4)A_{v,l} \tag{4.102}$$

4.15.2 Heat conduction model

An implicit one-dimensional, finite-difference scheme was used to calculate heat conduction through the ceiling, upper walls, lower walls and floor. This allows the temperature at any node to be calculated by solving a set of simultaneous equations for the unknown nodal temperatures at each time step [49]. The implicit method has the advantage of being unconditionally stable and therefore allows a larger timestep to be used in the calculations. The walls and ceiling may be specified as a single layer or as a two-layer system by including a substrate material. The floor is specified as a single layer.

The implicit form of the finite-difference scheme for a surface node is given by Incropera and deWitt [49] as:

$$(1 + 2\text{Fo})T_1^{p+1} - 2\text{Fo}T_2^{p+1} = \frac{2\text{FoBi}\dot{q}''}{h} + T_1^p \tag{4.103}$$

Where the Fourier and Biot numbers are given by:

$$\text{Fo} = \frac{\alpha\Delta t}{(\Delta x)^2} \text{ with } \alpha = \frac{k}{\rho c} \tag{4.104}$$

$$\mathrm{Bi} = \frac{h\Delta x}{k} \tag{4.105}$$

The implicit form for an interior node is given as:

$$-\mathrm{Fo}T_{m-1}^{p+1} + (1+2\mathrm{Fo})T_m^{p+1} - \mathrm{Fo}T_{m+1}^{p+1} = T_m^p \tag{4.106}$$

Writing an equation for each node gives n equations which must be solved simultaneously for each timestep. This can be done using the matrix inversion method by expressing the equations in the form [A][T]=[C], where:

$$[A] = \begin{bmatrix} 1+2\mathrm{Fo} & -2\mathrm{Fo} & 0 & 0 & \cdots & 0 \\ -\mathrm{Fo} & 1+2\mathrm{Fo} & -\mathrm{Fo} & 0 & \cdots & 0 \\ 0 & -\mathrm{Fo} & 1+2\mathrm{Fo} & -\mathrm{Fo} & \cdots & 0 \\ \vdots & \vdots & \ddots & \cdots & \cdots & \vdots \\ 0 & \cdots & \cdots & 0 & -2\mathrm{Fo} & 1+2\mathrm{Fo} \end{bmatrix} \tag{4.107}$$

$$[C] = \begin{bmatrix} 2\mathrm{FoBi}_{\mathrm{int}}\dot{q}''_{\mathrm{int}}/h + T_1^p \\ T_2^p \\ T_3^p \\ \vdots \\ 2\mathrm{FoBi}_{\mathrm{ext}}(T_{\mathrm{ext}} - T_n^p) + T_n^p \end{bmatrix} \tag{4.108}$$

$\dot{q}''_{\mathrm{int}}$ is the total heat flux incident on the interior surface. It includes both radiation (from the four wall radiation exchange model) and convection. A table of nodal temperatures may be compiled, starting with the prescribed initial conditions. The temperatures at the next timestep, [T], are found by multiplying the inverse matrix $[\mathrm{A}]^{-1}$ by the column vector [C] (Incropera and deWitt, [49]) using the method of LU decomposition [51]. An alternative method for solving the matrices using Gauss-Jordan elimination [13] is also available to the user.

4.15.3 Convective heat transfer coefficients

The interior heat transfer coefficient used in the heat transfer calculations between the gas layers and the room surfaces is calculated following the method described by Peacock et al [17] for the CFAST model.

The heat transfer coefficient (assuming natural convection) is given by:

$$h_c = \frac{k}{l} C_o (\mathrm{GrPr})^{1/3} \tag{4.109}$$

The characteristic dimension, l, is taken as $\sqrt{A_w}$ where A_w is the area of the surface in contact with the layer (upper or lower as applicable).

The Grashof number, Gr, is given as:

$$\mathrm{Gr} = \frac{gl^3 \mid T_g - T_s \mid}{\nu^2 T_g} \tag{4.110}$$

The thermal conductivity, k, of the gases is given by:

$$k = 2.72 \times 10^{-4} \left(\frac{T_g + T_s}{2} \right)^{4/5} \tag{4.111}$$

The kinematic viscosity, ν, of the gases is given by:

$$\nu = 7.18 \times 10^{-10} \left(\frac{T_g + T_s}{2} \right)^{7/4} \tag{4.112}$$

T_g and T_s are the temperatures of the gas layer and the wall or ceiling surface respectively, Pr is the Prandtl number (=0.72) and C_o is a coefficient which depends on orientation as given in Table 4.4.

Table 4.4: Surface coefficients

Orientation	**Coefficient,** C_o	**Condition**
vertical	0.13	all
horizontal	0.21	$T_g > T_s$
horizontal	0.012	$T_g < T_s$

The convective heat flux term is given by:

$$\dot{q}_c = h_c (T_g - T_s) A_s \tag{4.113}$$

4.16 Visibility

The mass fraction of soot in the upper layer is given by solving equations 4.8 and 4.9 for species generation at each time step. This requires a value for the soot yield (kg soot per kg of fuel pyrolysed) to be provided by the user. The mass concentration of soot in the upper layer (in kg of soot per m^3 of upper layer gas) is then given by:

$$C_{\mathrm{soot}} = Y_{\mathrm{soot}} \rho_u \tag{4.114}$$

The average extinction coefficient, k_{avg} (m^{-1}), is given by:

$$k_{\mathrm{avg}} = k_m C_{\mathrm{soot}} \tag{4.115}$$

where k_m is the specific extinction coefficient (m^2/kg soot) equal to 8790 for flaming combustion of ethene gas [52].

The maximum distance an observer can recognise an object, usually an exit sign, when viewing the object through smoke is defined as the visibility, V, by Beyler [25].

A study by Jin found that the product Vk_{avg} is a constant for a given object and lighting condition. The data correlated to a value of 3 for light-reflecting signs and 8 for light-emitting or illuminated signs [53]. The visibility is therefore given by:

$$V = \frac{3}{k_{\text{avg}}} \text{ metres (reflective signs)} \tag{4.116}$$

$$V = \frac{8}{k_{\text{avg}}} \text{ metres (illuminated signs)} \tag{4.117}$$

The program also calculates the optical density of each layer, OD (1/m), as a conversion of the extinction coefficient from natural log to base 10 units.

$$\text{OD} = \frac{k_{\text{avg}}}{2.3} \tag{4.118}$$

4.17 Toxicity of Combustion Products

Toxicity of combustion products is evaluated using the fractional effective dose (FED) method described by Purser [54]. The model evaluates the sum of the FED's at a specified height (in the upper or lower layer as applicable) for incapacitation due to carbon monoxide, and hypoxia (lack of oxygen) and also accounts for the accelerated breathing rate caused by exposure to carbon dioxide. The fractional effective dose FED is the ratio between the cumulative dose received after some time to the effective dose needed to cause incapacitation. An FED of 1 means that an incapacitation endpoint has been reached.

The model considers the time-dependent exposure of carbon monoxide in the upper layer by calculating a fractional effective dose for incapacitation using Stewart's equation (see Purser [55]) for the concentration of carboxyhemoglobin in the blood. RMV is the volume (in litres) of air breathed per minute and varies with the activity level.

$$\%\text{COHb} = (3.317 \times 10^{-5})(\text{ppm CO})^{1.036}(\text{RMV})t \tag{4.119}$$

$$\text{FED}_{\text{co}} = \frac{3.317 \times 10^{-5} \times \text{RMV}}{\%\text{COHb}} \int_0^t (\text{ppm CO})^{1.036} dt \tag{4.120}$$

The RMV in the expression for carbon monoxide FED is adjusted for the accelerated breathing rate caused by excess carbon dioxide as follows:

$$\text{RMV} = \exp(0.2486\%\text{CO}_2 + 1.9086) \tag{4.121}$$

The user may select an activity level appropriate to their analysis. The model uses values of RMV_o and incapacitation doses of COHb applicable to a 70 kg human, as shown in Table 4.5 [54].

Table 4.5: RMV and COHb incapacitation dose for different activity levels

Activity	RMV_o (l/min)	COHb Incapacitation Dose (%)
At Rest	8.5	40
Light Work	25	30
Heavy Work	50	20

Similarly, the FED for oxygen hypoxia is determined by evaluating the following integral from Purser [55].

$$\mathrm{FED}_{O_2} = \int_0^t \frac{1}{\exp(8.13 - 0.54(20.9\% - \%\mathrm{O_2}))} dt \tag{4.122}$$

Similarly, the FED for incapacitation by Hydrogen Cyanide (HCN) is determined by evaluating the following integral from Purser [55].

$$\mathrm{FED}_{HCN} = \int_0^t \frac{1}{\exp(5.396 - 0.023(\mathrm{ppmHCN}))} dt \text{ for HCN} > 80 \text{ ppm} \tag{4.123}$$

The model allows the user to select a height within the room at which to evaluate the incapacitation FED. The default is 2 m above the floor, a representative 'nose' height for an adult person. The total FED is therefore given by:

$$\mathrm{FED} = \mathrm{FED}_{O_2} + \mathrm{FED}_{CO} + \mathrm{FED}_{HCN} \tag{4.124}$$

The model uses a simple trapezoidal rule to evaluate the integrals using the upper layer species concentrations for the time when the layer interface is below the monitoring height selected by the user, and using the lower layer species concentrations for the time when the layer interface is above the monitoring height. The program only evaluates the integrals when the species concentrations are above initial ambient levels (or above 80 ppm in the case of HCN) and below ambient in the case of oxygen.

The user is also able to select a time-frame representing the period the room is occupied over which the FED is calculated. The default is for the entire simulation.

4.18 Thermal Radiation Effects

A thermal FED is calculated to account for the cumulative effects of thermal radiation received by a target (at the specified monitoring height above the floor). The radiation incident on the target is assumed to be due to a flat plate source at the layer interface height and at a temperature equal to the upper layer temperature T_u, and with emissivity equal to the upper layer emissivity ϵ_u. The configuration factor between the layer interface and the target is calculated for a flat surface and a parallel differential element [50]. The incident radiation is given by equation 4.125.

$$\dot{q}_{\rm rad} = \phi \epsilon_u \sigma T_u^4 \tag{4.125}$$

The fractional effective dose for thermal radiation is calculated from equation 4.126 from Clements and Gillespie [56] for the occupation period specified. The thermal radiation summation is only carried out at those time steps where the incident radiation exceeds an ambient threshold level of 1.7 kW/m^2.

$$\mathrm{FED}_{\rm rad} = \int_0^t \frac{1}{55(\dot{q}_{\rm rad} - 1.7)^{-0.8}} dt \tag{4.126}$$

4.19 Sprinkler and Thermal Detector Actuation

Sprinkler or detector actuation is predicted based on a single burning object located within the room of fire origin. There are two algorithms available for predicting sprinkler or thermal detector response. One uses Alpert's unconfined ceiling jet correlation as described by Evans [14] while the other uses the JET algorithm developed at NIST [57].

4.19.1 JET algorithm

The JET algorithm developed at NIST [57] predicts the plume centerline temperature, the ceiling jet temperature and the ceiling jet velocity produced by a single fire plume. The unique feature of this model is that the characteristics of the ceiling jet depend on the depth of the hot layer. The model assumes flames do not touch the ceiling and the fire is located near the centre of the compartment.

Variation of the ceiling jet temperature and velocity with distance below the ceiling is incorporated using the LAVENT method described in Appendix B NFPA 204 [58]. The ceiling jet temperature equals the ceiling surface temperature at the ceiling, and increases to a maximum value at a certain depth below the ceiling given by:

$$d_{\rm max} = 0.023 H (r/H)^{0.9} \text{ for } r/H > 0.2 \tag{4.127}$$

Thereafter the ceiling jet temperature reduces until it equals the upper layer temperature when above the layer interface height.

The differential equation describing the temperature of the sensing element is from Heskestad and Bill [59], and it incorporates both convective heating of the sensing element and conductive losses to the sprinkler piping. The equation is:

$$\frac{dT_e}{dt} = \frac{\sqrt{U_{\rm cj}}(T_{\rm cj} - T_e)}{\mathrm{RTI}} - \frac{C(T_e - T_{\rm int})}{\mathrm{RTI}} \tag{4.128}$$

For corner or wall fires, the heat release rate used in the ceiling jet correlation is modified asuming the method of reflection (i.e 4Q and 2Q for corner and wall fires respectively).

Based on comparisons with experimental data, the predictions of JET generally agreed with experimental results for compartments with ceiling heights up to 22 m [57].

4.19.2 Alpert's correlations

The correlations used for the temperature and velocity of the ceiling jet are those of Alpert as described by Evans [14] as follows:

$$T_{\mathrm{cj}} - T_{\mathrm{int}} = \frac{16.9\dot{Q}^{2/3}}{H^{5/3}} \quad \text{for} \quad \frac{r}{H} \leq 0.18 \tag{4.129}$$

$$T_{\mathrm{cj}} - T_{\mathrm{int}} = \frac{5.38(\dot{Q}/r)^{2/3}}{H} \quad \text{for} \quad \frac{r}{H} > 0.18 \tag{4.130}$$

$$U_{\mathrm{cj}} = 0.96\left(\frac{\dot{Q}}{H}\right)^{1/3} \quad \text{for} \quad \frac{r}{H} \leq 0.15 \tag{4.131}$$

$$U_{\mathrm{cj}} = \frac{0.195\dot{Q}^{1/3}H^{1/2}}{r^{5/6}} \quad \text{for} \quad \frac{r}{H} > 0.15 \tag{4.132}$$

These correlations are for the maximum temperature and velocity in an unconfined ceiling jet, so it is assumed that the detector/sprinkler link is located at the distance below the ceiling at which these maximum values occur.

Once again, equation 4.128 gives a differential equation describing the temperature of the sensing element.

For corner or wall fires, the heat release rate used in the ceiling jet correlation is modified asuming the method of reflection (i.e 4Q and 2Q for corner and wall fires respectively).

4.19.3 Sprinkler suppression

The effect of the sprinkler on the fire may be modelled using a sprinkler fire suppression algorithm developed by Evans [60]. Alternatively, the user may select a fire control option which will maintain the fire size at a constant heat release rate equal to the fire size at the time of sprinkler activation. The fire suppression algorithm developed by Evans for unshielded furniture fires is:

$$\dot{Q}(t - t_{\mathrm{act}}) = \dot{Q}(t_{\mathrm{act}})\exp\left[\frac{-(t - t_{\mathrm{act}})}{3(\dot{w}''^{-1.85})}\right] \tag{4.133}$$

$\dot{w}''$ is the water spray density (mm/s), t_{act} is the sprinkler activation time (s) and $\dot{Q}(t_{\mathrm{act}})$ is the heat release rate of the fire at the time of sprinkler activation (kW).

4.20 Smoke Detector Actuation

Smoke detector response is based on the calculated smoke optical density at the location of the detector. The response time of the detector is calculated using Heskestad's method [61], while the smoke concentration in the ceiling jet and hence optical density is calculated using a method developed by Davis et al [62].

The response time of the detector is given by:

$$\frac{dD_t}{dt} = \frac{1}{\tau}(D_o - D_i) \tag{4.134}$$

$$\tau = \frac{l}{u} \tag{4.135}$$

where D_o is the optical density outside the detector, D_i is the optical density inside the detector chamber and τ is a time constant for the detector, l is the characteristic length of the detector and u is the velocity of the ceiling jet at the location of the detector.

Davis et al [62] uses the concept of a substitute source in his development of a correlation for the smoke concentration in the ceiling jet. The ceiling jet is considered to be submerged within the hot gas layer, and thus will be hotter than the case where the hot layer is not present. The substitute source is described by a heat release rate $\dot{Q}_2$ and location beneath the ceiling H_2. $\dot{Q}_2$ is given by:

$$\dot{Q}_2^* = \left[\frac{D\dot{Q}_1^{*2/3} - C_L(1 + K\dot{Q}_1^{*2/3})}{D + C_L K(1 + K\dot{Q}_1^{*2/3})}\right]^{3/2} \tag{4.136}$$

$$\dot{Q}_1^* = \frac{\dot{Q}}{\rho_l c_p T_l \sqrt{g}(Z - z_o)^{5/2}} \tag{4.137}$$

where $K = 9.1(1 - \lambda_r)^{2/3}$; $C_L = Y_s \rho_u$ is the scalar concentration of smoke in the upper layer; Z is the layer height above the fire while z_o is the location of the virtual point source.

The location of the substitute source Z_2 is given by:

$$\dot{Z}_2 = Z_1 \left[\frac{\dot{Q}_1^*}{\dot{Q}_2^* + \frac{(\lambda^2+1)}{\lambda^2}\frac{C_L}{D}(1 + K\dot{Q}_2^{*2/3})\dot{Q}_2^{*1/3}}\right]^{2/5} \tag{4.138}$$

$$D = \frac{Y_s \frac{(\lambda^2+1)}{\lambda^2}\rho_l c_p T_l}{3.4 h_c \pi (1 - \lambda_r)^{1/3}(1.201)^2(0.12)^2} \tag{4.139}$$

$$H_2 = H_1 - Z_1 + Z_2 \tag{4.140}$$

The maximum concentration at the ceiling on the plume centreline is:

$$C_{spo} = \frac{D\dot{Q}_2^{*2/3}\left(\frac{Z_2}{H_2}\right)^{5/3}}{1 + K\dot{Q}_2^{*2/3}\left(\frac{Z_2}{H_2}\right)^{5/3}} + C_L \tag{4.141}$$

The maximum concentration in the ceiling jet at $r = 0.18H$ is:

$$C_{so} = \sqrt{2}\frac{\lambda^2}{\lambda^2 + 1}(C_{spo} - C_L) + C_L \tag{4.142}$$

Finally, the maximum smoke concentration in the ceiling jet at a radial distance of r from the plume centreline (where $r > 0.18H$) is given by:

$$C_{so}(r) = (C_{so} - C_L)\left(\frac{0.18H}{r}\right)^{0.57} + C_L \tag{4.143}$$

A fuller derivation of the above equations is given by Davis et al [62].

A further refinement is introduced to account for a variation in the velocity of the ceiling with distance below the ceiling. The maximum gas temperature and velocity (and smoke concentration) typically occurs at about 1% of the fire-ceiling height below the ceiling. The ceiling jet velocity affects equation 4.135 for the time constant and subsequently the rate of change of optical density. Variation of the ceiling jet velocity with distance below the ceiling is incorporated using the LAVENT method described in Appendix B NFPA 204 [58]. This modification only affects calculations where the smoke optical density inside the detector is of interest. The calculated optical density outside the detector is a maximum and does not change with distance beneath the ceiling for a given radial distance from the plume centreline. Gas transit times for the heat front to reach the detector are not considered.

The optical density limits for actuation are based on AS 1603.2 [63] test limits as described in the Australian Fire Engineering Guidelines [64]. Three sensitivity classes are given: normal, high and very high with optical density limits of 0.097, 0.055 and 0.013 m^{-1} respectively. These limits are applicable to photoelectric detectors, but are expected to be conservative if applied to ionisation detectors in flaming fires.

For smoke detectors located outside the room or fire origin, there is no ceiling jet and therefore no dependence on radial distance. In this case, the average upper layer optical density in the room is compared to the optical density required for response to determine when the detector activates.

4.21 Numerical Solution

There are seventeen ordinary first-order differential equations which are solved using a stiff differential equation solver. The numerical solution was from that provided in a mathematics library, BNALib [13]. The seventeen equations relate to upper layer volume, upper and lower layer temperature, oxygen, soot, unburned fuel, water vapor,

carbon monoxide and carbon dioxide concentrations, and finally the sprinkler/detector link temperature.

The numerical solver comprises an adaptive driver that estimates the error and adapts the step size to achieve the specified accuracy. An initial timestep of 1 second is generally used, which the solver will reduce as necessary. The default error tolerance is 0.1.

The flame spread ODE equations for upward and lateral spread are solved using a fourth order Runge Kutta technique [13].

4.22 Programming Language

The model described in this report was programmed using Microsoft Visual Basic Version 6.0. The software is designed to run under the Microsoft Windows 95, 98, 2000, XP or NT 3.51 environment or later.

Section 5

Material Property Data

5.1 Method of Grenier and Janssens

5.1.1 Input of data for the wall/ceiling materials

The user supplies information about the lining material from cone calorimeter tests. The test heat flux, the time to ignition, and the peak heat release rate achieved are required. The model will then correlate the ignition data to estimate the ignition temperature and effective thermal inertia, and will correlate the peak heat release rate to estimate the heat of gasification. Data measured at a minimum of three external heat fluxes are required, although a greater number of external heat fluxes are preferred. The method used is described below.

5.1.2 Ignition temperature and thermal inertia

The procedure for determining the surface temperature for ignition T_{ig} and the effective thermal inertia $k\rho c$ from cone calorimeter measurements is taken from Grenier [11] and Janssens [65, 66].

1. Samples are tested at a range of different irradiance levels (at least three). Ideally there should be replicates tested at each irradiance. The average time to ignition, t_{ig}, for each heat flux is determined. Taking the time to ignition, t_{ig} as the time for the heat release rate to reach 30 kW/m^2 agreed reasonably well with the observed ignition times.

2. Correlate the ignition times by plotting $[1/t_{ig}]^n$ on the Y-axis versus $\dot{q}''_e$ on the X-axis. Determine the value of n that results in the highest correlation coefficient (R^2), allowing n to be in the range 0.547 to 1.

3. Determine the X-intercept from a straight line fit through the data. The X-intercept is taken as the critical heat flux for ignition $\dot{q}''_{cr}$.

4. Solve (by iteration) the following equation for the surface temperature for ignition, T_{ig}, taking the convective heat transfer coefficient $h_c = 0.0135$ kW/m^{2}K, and surface emissivity at ignition, ϵ, as appropriate for the material.

$$\epsilon \dot{q}''_{cr} = h_c(T_{ig} - T_\infty) + \epsilon\sigma\left(T_{ig}^4 - T_\infty^4\right) \tag{5.1}$$

5. Solve the following equation for the total heat transfer coefficient for the surface at ignition.

$$h_{ig} = \frac{\epsilon \dot{q}''_{cr}}{(T_{ig} - T_\infty)} \tag{5.2}$$

6. Plot the ignition data again, this time assuming thermally thick behaviour and using n=0.547. Include the data point $\dot{q}''_{cr}$ from above, on the X-axis.

7. Determine the slope of a straight line drawn through two points. The $\dot{q}''_{cr}$ from above on the X-axis and the data point for the highest heat flux. This is a simplification to make the calculation easier.

8. Compute the apparent thermal inertia, $k\rho c$ as:

$$k\rho c = h_{ig}^2 \left[\frac{1}{0.73b\dot{q}''_{cr}}\right]^{1.828} \tag{5.3}$$

5.1.3 Heat of gasification

The heat of gasification for the material is determined from a correlation of the peak rate of heat release from cone calorimeter tests following the methodology of Quintiere [5]. The cone test results will also provide the effective heat of combustion, ΔH_c (kJ/g). This is required for the following procedure.

1. Correlate the peak heat release rate by plotting $\dot{q}''_{peak}$ on the Y-axis versus $\dot{q}''_e$ on the X-axis.

2. Determine the slope of a linear regression line through the data.

3. Calculate the heat of gasification L_g as follows.

$$L_g = \frac{\Delta H_c}{\text{slope}} \tag{5.4}$$

5.1.4 Example

A material has been tested in a cone calorimeter with the results shown in Table 5.1. The average effective heat of combustion for the material was determined to be 13 kJ/g.

Correlate the ignition times by plotting $[1/t_{ig}]^n$ on the Y-axis versus $\dot{q}''_e$ on the X-axis as shown in Figure 5.1. By trial and error the value of n that resulted in the highest

Table 5.1: Summary of data from cone calorimeter tests

Heat Flux (kW/m^2)	Time to Ignition (s)	Peak HRR (kW/m^2)
50	12	137.9
35	19	106.7
25	33	90.0

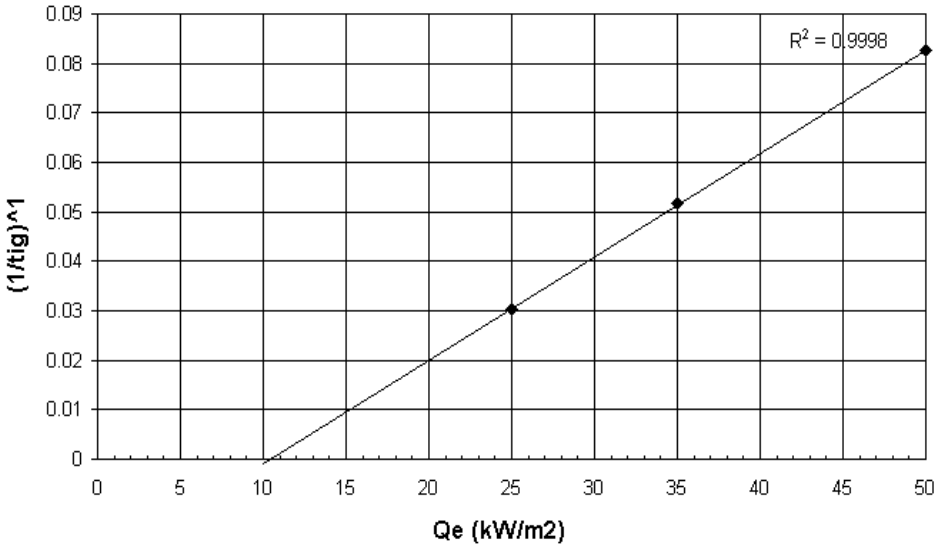

Figure 5.1: Correlation of ignition times for best-fit "n"

correlation coefficient (R^2), and in the range 0.547 to 1 was 1. This indicates thermally thin behaviour.

Determine the X-intercept from a straight line fit through the data. The X-intercept is taken as the critical heat flux for ignition $\dot{q}''_{\rm cr}$ and here is determined to be 10.4 kW/m^2.

Solve (by iteration) the following equation for the surface temperature for ignition, $T_{\rm ig}$, taking the convective heat transfer coefficient $h_{\rm c} = 0.0135$ kW/m^{2}K, and surface emissivity $\epsilon = 0.88$, $T_\infty = 293$ K and $\dot{q}''_{\rm cr} = 10.4$.

$$\epsilon \dot{q}''_{\rm cr} = h_{\rm c}(T_{\rm ig} - T_\infty) + \epsilon\sigma\left(T_{\rm ig}^4 - T_\infty^4\right)$$

$T_{\rm ig}$ is determined to be 307°C.

Solve the following equation for the total heat transfer coefficient (kW/m^{2}K) for the surface at ignition:

$$h_{\rm ig} = \frac{\epsilon \dot{q}''_{\rm cr}}{(T_{\rm ig} - T_\infty)} = \frac{0.88 \times 10.4}{(307 - 20)} = 0.032$$

Plot the ignition data again, this time assuming thermally thick behaviour and using n=0.547 and including the data point $\dot{q}''_{\rm cr}$ from above, on the X-axis as shown in Figure 5.2. Determine the slope of the (dashed) line drawn through the highest and lowest points.

$$\text{slope} = \frac{(1/12)^{0.547}}{(50 - 10.4)} = 0.00645$$

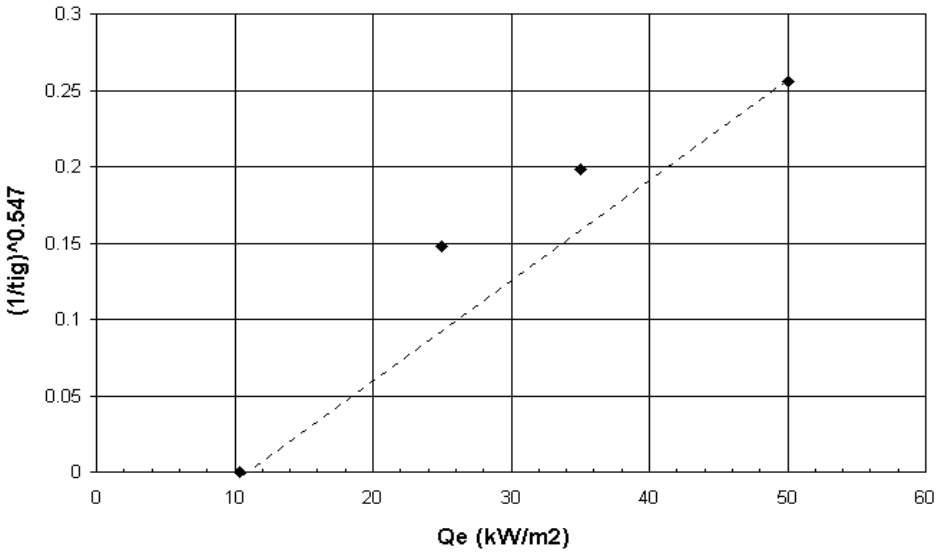

Figure 5.2: Correlation of ignition times for "n=0.547"

Compute the apparent thermal inertia, $k\rho c$ as:

$$k\rho c = h_{\text{ig}}^2 \left[\frac{1}{0.73 b \dot{q}''_{\text{cr}}}\right]^{1.828} = (0.032)^2 \left[\frac{1}{0.73(0.00645)(10.4)}\right]^{1.828} = 0.253$$

Correlate the peak heat release rate by plotting $\dot{q}''_{\text{peak}}$ on the Y-axis versus $\dot{q}''_{\text{e}}$ on the X-axis as shown in Figure 5.3. The slope of the linear regression line is found to be 1.93.

Calculate the heat of gasification L_{g}.

$$L_{\text{g}} = \frac{\Delta H_{\text{c}}}{\text{slope}} = \frac{13}{1.93} = 6.7 \text{ kJ/g}$$

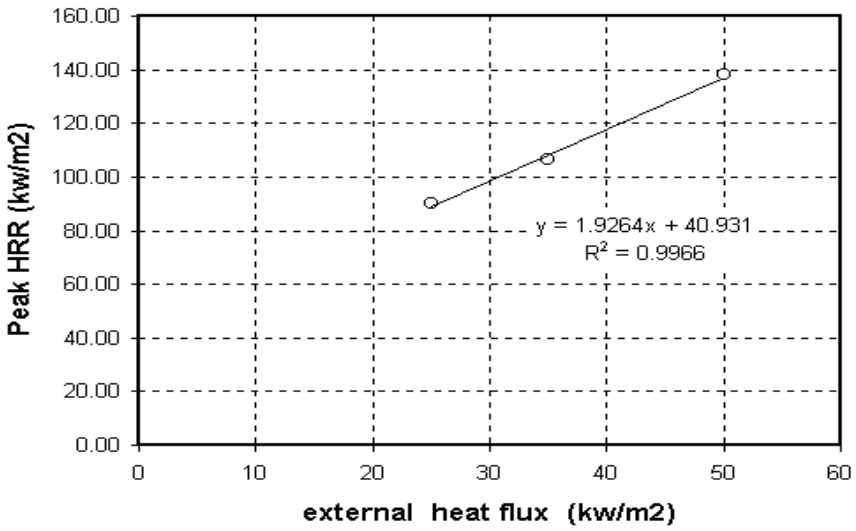

Figure 5.3: Correlation of peak heat release rates

5.2 Flux Time Product Method

The Flux Time Product (FTP) method is described by Silcock and Shields [10]. They correlated the ignition data assuming a power law expression based on physically consistent dimensionless groups to give the following.

$$(\dot{q}''_{\mathrm{e}} - \dot{q}''_{\mathrm{cr}})^n t_{\mathrm{ig}} = FTP_n \text{ for } n \geq 1 \tag{5.5}$$

FTP is the flux time product and n is the flux time product index. Rearranging equation 5.5 gives:

$$\dot{q}''_{\mathrm{e}} = \dot{q}''_{\mathrm{cr}} + \frac{FTP_n^{1/n}}{t_{\mathrm{ig}}^{1/n}} \tag{5.6}$$

This represents a straight line by plotting time to ignition raised to the power 1/n against the externally applied heat flux. The value of n resulting in the best fit is determined with n in the range 1 (thermally thin) to 2 (thermally thick). The FTP_n can then be determined from the slope of the line.

$$FTP_n = (\mathrm{slope})^{\mathrm{n}} \tag{5.7}$$

Then for any specified external heat flux, the time to ignition is given by rearranging equation 5.5, and this is equivalent to equation 3.23 with n=1/p.

$$t_{\mathrm{ig}} = \frac{FTP_n}{(\dot{q}''_{\mathrm{e}} - \dot{q}''_{\mathrm{cr}})^n} \tag{5.8}$$

The flux time product method does not require the effective thermal inertia to be determined.

Section 6

Conclusions

BRANZFIRE is a zone model used to determine the flow of smoke and gases and its properties through a building. BRANZFIRE is based on a set of differential equations that predict state variables using enthalpy and mass flux over small time steps. These equations are derived from the conservation of energy and mass and the ideal gas law. Therefore the main contributions to any errors or differences that exist between the model predictions and real life or full-scale experiments are due to the many simplifying assumptions that must be made.

BRANZFIRE has been subjected to a limited number of comparisons to experimental data for compartment fires with reasonable agreement [67]. Because BRANZFIRE is a collection of many different inter-related algorithms it is a huge task to provide comprehensive validation information covering all the features provided. However, many of the underlying algorithms used have been previously published by others in the literature. Verification of BRANZFIRE is intended to be an ongoing process with additional data and comparisons with experiments continuing in the future.

It is important that users be familiar with the underlying physics and assumptions on which the program is based in order to be able to critically evaluate the results obtained.

BRANZ Ltd takes no responsibility for any loss or design resulting from the use of this program, whether proper or not. All responsibility lies with the end user, who shall decide on the validity of any results obtained using BRANZFIRE and who shall exercise caution when applying the results to any particular situation.

References

[1] Colleen Wade. A Room Fire Model Incorporating Fire Growth on Combustible Lining Materials. Master's thesis, Worcester Polytechnic Institute, Worcester, MA, April 1996.

[2] Colleen Wade and Jonathan Barnett. A room-corner model including fire growth on linings and enclosure smoke-filling. *Journal of Fire Protection Engineering*, 8(4):27–36, 1997.

[3] C.A. Wade, D. LeBlanc, J. Ierardi, and J.R. Barnett. A room-corner fire growth and zone model for lining materials. In *Second International Conference of Fire Research and Engineering*, 1997.

[4] Colleen Wade. A new engineering tool for evaluating the fire hazard in rooms. In *Proceedings of the Building Control Commission International Convention*, April 1999.

[5] James G. Quintiere. A simulation model for fire growth on materials subject to a room-corner test. *Fire Safety Journal*, 20:313–339, 1993.

[6] International Organization for Standardization. Room fire test in full scale for surface products (ISO 9705), 1993.

[7] Brian Y. Lattimer. *SFPE Handbook of Fire Protection Engineering Third Edition*, chapter 14 Section 2 Heat Fluxes from Fires to Surfaces. National Fire Protection Association, Quincy, 2002.

[8] Gunnar Heskestad. Engineering relations for fire plumes. *Fire Safety Journal*, 7:25–32, 1984.

[9] G. Back, C. Beyler, P. DiNenno, and P. Tatem. Wall incident heat flux distributions resulting from an adjacent fire. In Takashi Kashiwagi, editor, *Fire Safety Science - Proceedings of the Fourth International Symposium*, 1994.

[10] G. W. H. Silcock and T. J. Shields. A protocol for analysis of time-to-ignition data from bench scale tests. *Fire Safety Journal*, 24:75–95, 1995.

[11] A.T. Grenier and M.L. Janssens. An improved method for analyzing ignition data of composites. In *Proceedings of the International Conference on Fire Safety Vol 23*, 1997.

[12] Marc Janssens, Ondrej Grexa, Mark Dietenberger, and Robert White. Predictions of ISO 9705 Room/Corner Test Using a Simple Model. In *Conference Proceedings of 4th International Fire and Materials Conference*. Interscience Communications Limited, 1995.

[13] C. David Eagle Jr. BNALib A Basic Numerical Analysis Library for Personal Computers. Technical report, 1997.

[14] D. D. Evans. *Handbook of Fire Protection Engineering*, chapter 9 section 1 Ceiling Jet Flows. National Fire Protection Association, 1988.

[15] Matti Kokkala, Djebar Baroudi, and William J. Parker. Upward flame spread on wooden surface products: Experiments and numerical modelling. In Yuji Hasemi, editor, *Fire Safety Science - Proceedings of the Fifth International Symposium*. International Association for Fire Safety Science, 1997.

[16] American Society for Testing and Materials. ASTM E 1321-90 Standard test method for determining material ignition and flame spread properties, 1990.

[17] Richard D. Peacock, Glenn Forney, Paul A. Reneke, Rebecca Portier, and Walter W. Jones. CFAST, the Consolidated Model of Fire and Smoke Transport. NIST Technical Note 1299, National Institute of Standards and Technology, February 1993.

[18] B.V. Karlekar. *Thermodynamics for Engineers*. Prentice-Hall, Inc., Englewood Cliffs, N.J., 1983.

[19] G. F. C. Rogers and Y. R. Mayhew. Thermodynamic and Transport Properties of Fluids SI Units, 1992.

[20] J. A. Ierardi. A guide for specifying combustion chemistry rations in the cfast and fastlite zone models.

[21] William M. Pitts. The global equivalence ratio concept and the prediction of carbon monoxide formation in enclosure fires. NIST Monograph 179, National Institute of Standards and Technology, June 1994.

[22] A. Tewarson, F.H. Jiang, and T. Morikawa. Ventilation controlled combustion of polymers. *Combustion and Flame*, 95:151–169, 1993.

[23] Archibald Tewarson. *SFPE Handbook of Fire Protection Engineering*, chapter 4 Section 3 Generation of Heat and Chemical Compounds in Fires. National Fire Protection Association, 3rd edition, 2002.

[24] Daniel T. Gottuk. Generation of carbon monoxide in compartment fires. Technical Report NIST-GCR-92-619, National Institute of Standards and Technology, Washington DC, 1992.

[25] C. Beyler. *Fire Dynamics and Chemistry: An Engineering Approach (Draft)*. Worcester Polytechnic Institute, 1988.

[26] B. J. McCaffrey. Momentum implications for buoyant diffusion flames. *Combustion and Flame*, 52:149, 1983.

[27] Björn Karlsson and James G. Quintiere. *Enclosure Fire Dynamics*. CRC Press, 2000.

[28] J. Quintiere and B. McCaffrey. The burning of wood and plastic cribs in an enclosure: Volume 1. Technical Report NBSIR 80-2054, National Bureau of Standards, Washington DC, 1980.

[29] John A. Rockett. Fire induced gas flow in an enclosure. *Combustion Science & Technology*, 12:165–175, 1976.

[30] Marc Janssens. *Heat Release in Fires*, chapter 6a Room Fire Models. Elsevier Applied Science, 1992.

[31] David M. Birk. *An Introduction to Mathematical Fire Modeling*. Technomic Publishing Company, 1991.

[32] Howard W. Emmons. *Handbook of Fire Protection Engineering*, chapter 8 section 1 Vent Flows. National Fire Protection Association, Quincy, 1988.

[33] Vytenis Babrauskas and Robert Brady Williamson. Post-flashover compartment fires: Basis of a theoretical model. *Fire and Materials*, 2(2):39–53, 1978.

[34] Leonard Y. Cooper and Glenn P. Forney. The Consolidated Compartment Fire Model (CCFM) Computer Code Application CCFM.VENTS - Part I: Physical Basis. NISTIR 4342, National Institute of Standards and Technology, 1990.

[35] Glenn P. Forney and Leonard Y. Cooper. The Consolidated Compartment Fire Model (CCFM) Computer Code Application CCFM.VENTS - Part II: Software Reference Guide. NISTIR 4343, National Institute of Standards and Technology, 1990.

[36] Leonard Y. Cooper and Glenn P. Forney. The Consolidated Compartment Fire Model (CCFM) Computer Code Application CCFM.VENTS - Part III: Catalog of Algorithms and Subroutines. NISTIR 4344, National Institute of Standards and Technology, 1990.

[37] Glenn P. Forney, Leonard Y. Cooper, and William F. Moss. The Consolidated Compartment Fire Model (CCFM) Computer Code Application CCFM.VENTS - Part IV: User Reference Guide. NISTIR 4345, National Institute of Standards and Technology, 1990.

[38] Leonard Y. Cooper. VENTCF2: an Algorithm and Associated FORTRAN 77 Subroutine for Calculating Flow through a Horizontal Ceiling/Floor Vent in a Zone-type Compartment Fire Model. *Fire Safety Journal*, 28:253–287, 1997.

[39] C Huggett. Estimation of rate of heat release by means of oxygen consumption measurements. *Fire and Materials*, 4:61–65, 1980.

[40] H. E. Nelson. FPETOOL - Fire protection tools for hazard estimation. NISTIR 4380, National Institute of Standards and Technology, 1990.

[41] Ross Parry, Colleen Wade, and Michael Spearpoint. Implementing a glass fracture module in the branzfire zone model. *Journal of Fire Protection Engineering*, 13:157–183, 2003.

[42] Ross Parry. Implementation of a glass fracture module for the BRANZfire compartment fire zone modelling software. Master's thesis, University of Canterbury, Department of Civil Engineering, Christchurch, New Zealand, 2002.

[43] P. E. Sincaglia and J. R. Barnett. Development of a glass window fracture model for zone-type computer fire codes. *Journal of Fire Protection Engineering*, 8:101–118, 1997.

[44] P. J. Pagni and A. A. Joshi. Glass breaking in fires. In Geoffrey Cox and Brian Langford, editors, *Fire Safety Science - Proceedings of the Third International Symposium*. Elsevier Applied Science, 1991.

[45] M. J. Skelly, R. J. Roby, and C. L. Beyler. An experimental investigation of glass breakage in compartment fires. *Journal of Fire Protection Engineering*, 3:25–34, 1991.

[46] Leonard Y. Cooper. *SFPE Handbook of Fire Protection Engineering Third Edition*, chapter 9 Section 3 Smoke and Heat Venting. National Fire Protection Association, Quincy, 2002.

[47] Craig Beyler. *SFPE Handbook of Fire Protection Engineering Third Edition*, chapter 7 Section 2 Flammability Limits of Premixed and Diffusion Flames. National Fire Protection Association, Quincy, 2002.

[48] Glenn P. Forney. Computing radiative heat transfer occurring in a zone model. *Fire Science & Technology*, 14:31–47, 1994.

[49] Frank P. Incropera and David P. De Witt. *Fundamentals of Heat and Mass Transfer*. John Wiley and Sons, 1990.

[50] C.L. Tien, K.Y. Lee, and A.J. Stretton. *Handbook of Fire Protection Engineering*, chapter 4 section 1 Radiation Heat Transfer. National Fire Protection Association, 1995.

[51] Martin Block, Dr Sami Shakir, and John Smith. ProMath 2.0 and ProMath/VB 2.0 dual version. Professional BASIC Mathematics Library, 1993.

[52] George W. Mulholland and Mun H. Choi. Measurement of the specific extinction coefficient for acetylene and ethene smoke using the large agglomorate optics facility. In *Twenty-Seventh Symposium (International) on Combustion*, pages 1515–1522. The Combustion Institute, 1998.

[53] George W. Mullholland. *SFPE Handbook of Fire Protection Engineering*, chapter 15 section 2 Smoke Production and Properties. National Fire Protection Association, 2nd edition, 1995.

[54] D. Purser. *Handbook of Fire Protection Engineering*, chapter 14 Section 1 Toxicity Assessment of Combustion Products. National Fire Protection Association, Quincy, 1988.

[55] David A. Purser. *SFPE Handbook of Fire Protection Engineering Third Edition*, chapter 6 Section 2 Toxicity Assessment of Combustion Products. National Fire Protection Association, Quincy, 2002.

[56] P.A. Clements and D. Gillepsie. Egress constraints on occupants when subjected to radiant energy. In D. P. Lund and E. A. Angell, editors, *Proceedings International Conference on Fire Research and Engineering (ICFRE).*, 1995.

[57] William D. Davis. Zone fire model jet: A model for the prediction of detector activation and gas temperature in the presence of a smoke layer. NISTIR 6324, National Institute of Standards and Technology, May 1999.

[58] National Fire Protection Association. Guide for smoke and heat venting (NFPA 204), 1998.

[59] Gunnar Heskestad and Jr Robert G. Bill. Quantification of thermal responsiveness of automatic sprinklers including conduction effects. *Fire Safety Journal*, 14:113–125, 1988.

[60] David E Evans. Sprinkler fire suppression algorithm for HAZARD. In *Proceedings of the 12th Joint Panel Meeting of the UJNR Panel on Fire Research and Safety, Oct 27 - Nov 2, 1992*, 1994.

[61] G. Heskestad. Generalized characteristics of smoke entry and response for products-of-combustion detectors. In *Proceedings, 7th International Conference on Problems of Automatic Fire Detection*. Rheinish-Westfalischen Technischen Hochschule, Aachen, Germany, 1975.

[62] William D. Davis, Thomas Cleary, Michelle Donnelly, and Samuel Hellerman. Predicting smoke and carbon monoxide detector response in the ceiling jet in the presence of a smokelayer. NISTIR 6976, National Institute of Standards and Technology, 2003.

[63] Standards Australia. AS 1603 Automatic Fire Detection and Alarm Systems - Part 2: Point Type Smoke Detectors, 1989.

[64] Fire Code Reform Centre. Fire engineering guidelines, 1996.

[65] Marc Janssens. Piloted ignition of wood: A review. *Fire and Materials*, 15:151–167, 1991.

[66] Marc Janssens. *Heat Release in Fires*, chapter 9 Determining Flame Spread Properties From Cone Calorimeter Measurements. Elsevier Applied Science, 1992.

[67] C. A. Wade. BRANZFIRE 2004 Compilation of verification data, 2004.

Appendix A

Format of Cone Data File

An example of a ".txt" file for including the material cone calorimeter data is given here. Note comments are given in bold. They are not part of the file.

```
"EUMAT6 material"
"Number of HRR Curves",4
"Heat Flux",25
```

Input a single heat release rate curve for the material starting from the lowest external heat flux.

```
"Number of HRR Data Pairs",20
"sec,kw/m2"
```

The number of data pairs must correspond to the number given above (20).

```
0,34.4
5,54.7
10,64.5
15,63.7
20,53.1
25,33.1
...
```

Repeat for next heat flux.

```
"Heat Flux",35
"Number of HRR Data Pairs",27
"sec,kw/m2"
0,44.4
5,95.3
10,104.7
15,91.6
20,76.4
```

```
25,62.1
...
”Heat Flux”,50
”Number of HRR Data Pairs”,37
”sec,kw/m2”
0,73.1
5,127.4
10,128.5
15,121.2
20,106
25,92
...
”Heat Flux”,75
”Number of HRR Data Pairs”,34
”sec,kw/m2”
0,36.1
5,73.5
10,75
15,73.7
20,60.4
25,47.8
...
”Ignition Data”
”Number of Pairs”,8
”flux kw/m2,ignition time sec, peak hrr kw/m2”
```

Number of entries corresponds to number given above (8). Enter lowest to highest external flux.

```
25,65,75.2
25,65,64.5
35,35,95.6
35,30,104.7
50,15,151.9
50,10,128.5
75,5,85.4
75,5,75
”Flame Spread Parameter”,0
”Min Surface Temp For Spread”,0
”Effective Heat of Combustion”,0
```

If number of pairs is set to zero, the user can enter ignition temperature, thermal inertia, heat of gasification, area under the heat release rate curve, and critical flux directly as follows.

```
 ...
”Number of Pairs”, 0
”Ignition Temperature”, 740
”Thermal Inertia”, 0.366
```

```
"Heat of Gasification",0.72
"Area under Curve", 2359
"Critical Flux", 22
```

If the area under the curve is entered as zero, then the area will be automatically calculated using the rate of heat release curve supplied.

Appendix B

List of Model Constants

Constants used in the model are given in Table B.1.

Parameter	Description	Value	Units
A	plume entrainment coefficient	0.076	
C_d	discharge coefficient	0.68	
c_p	specific heat of air at constant pressure	1.005	kJ kg^{-1} K^{-1}
g	acceleration due to gravity	9.807	m sec^{-2}
h_{ext}	exterior convective heat transfer coefficient	5	W m^{-2} K^{-1}
M_{air}	molecular weight of air	29	
M_{CO_2}	molecular weight of carbon dioxide	44	
M_{CO}	molecular weight of carbon monoxide	28	
M_{H_2O}	molecular weight of water	18	
M_{O_2}	molecular weight of oxygen	32	
M_{N_2}	molecular weight of nitrogen	28	
P	atmospheric pressure	101.325	kPa
R	Universal Gas Constant	8314.34	J $kmol^{-1}K^{-1}$
R_{air}	Gas Constant Air	0.2871	kJ kg^{-1} K^{-1}
T_f	flame temperature	1250	K
T_∞	reference temperature of air	288.15	K
$Y_{O_2}\infty$	mass fraction of oxygen in ambient air	0.2313	
$Y_{CO_2}\infty$	mass fraction of carbon dioxide in ambient air	0.005	
ρ_∞	reference density of air	1.225	kg m^{-3}
π	pi	3.14159265	
γ	ratio of specific heats	1.4	
σ	Stefan Boltzmann Constant	5.66961E-08	$Wm^{-2}K^{-4}$
ΔH_{air}	energy release per mass of air consumed	3	kJ g^{-1}

Table B.1: Constants used in BRANZFIRE Model